(NASA-CR-4141) TURBULENT FLOW IN A 180 DEG BEND: MODELING AND COMPUTATIONS Final Report (Sterling Federal Systems) 51 p CSCL 20D

N89-24579

Unclas

H1/34 0217935

NASA Contractor Report 4141

Turbulent Flow in a 180° Bend: Modeling and Computations

Upender K. Kaul
Sterling Federal Systems, Inc.
Palo Alto, California

Prepared for
Ames Research Center
under Contract NAS2-11555

National Aeronautics and
Space Administration
Office of Management
Scientific and Technical
Information Division

1989

TABLE OF CONTENTS

	Page
ABSTRACT	1
INTRODUCTION	1
TURBULENCE MODEL	2
CURVATURE CORRECTION	11
NUMERICAL METHOD	11
DISCUSSION OF RESULTS	12
CONCLUDING REMARKS	16
REFERENCES	19
APPENDIX: USER MANUAL FOR KEM CODE	43

PRECEDING PAGE BLANK NOT FILMED

PAGE 11 INTENTIONALLY BLANK

LIST OF FIGURES

Figure	Title	Page
1.	Variation of turbulence kinetic energy from the wall to the center-line for a coarse grid	23
2.	Variation of dissipation rate from the wall to to the center-line for a coarse grid	24
3.	Distribution of turbulence kinetic energy from the wall to the center-line for a fine grid	25
4.	Distribution of dissipation rate from the wall to the center-line for a fine grid	26
5.	Near-wall variation of turbulence kinetic energy with the wall variable, y^+, for a coarse grid	27
6.	Near-wall variation of Reynolds stress with the wall variable, y^+, for a fine grid	28
7.	Distribution of turbulence kinetic energy from the wall to the center-line for a coarse grid and length scale distribution B	29
8.	Grid for a Two-Dimensional U-Bend (180° Curved Duct)	30
9.	Streamfunction Contours in the U-Bend	31
10.	Cross-Flow Variation of Mean Streamwise Velocity at Various Angular Locations	32
11.	Turbulence Kinetic Energy Contours in the U-Bend	33
12.	Cross-Flow Variation of Turbulence Kinetic Energy at Various Angular Locations	34
13.	Cross-Flow Variation of Turbulence Viscosity	

PRECEDING PAGE BLANK NOT FILMED

PAGE IV INTENTIONALLY BLANK

at Various Angular Locations 35

14. Cross-Flow Variation of Turbulence Shear Stress at Various Angular Locations 36

15. Variation of Skin Friction Along the Inner and Outer Walls 37

16. Comparison Between Predictions and Experimental Data for Mean Streamwise Velocity at Various Sections Around the Bend 38-41

A-1. Convergence History of the KEM Code Corresponding to Wall Function and Wall Boundary Condition Approaches 42

ABSTRACT

A low Reynolds number k - ϵ turbulence model has been presented which yields accurate predictions of the kinetic energy near the wall. The model is validated with the experimental channel flow data of Kreplin and Eckelmann. The predictions are also compared with earlier results from direct simulation of turbulent channel flow. The model is especially useful for internal flows where the inflow boundary condition on ϵ is not generally easily prescribed. The model partly derives from some observations based on earlier direct simulation results of near-wall turbulence. Very near the wall, limiting behavior on the turbulence kinetic energy and the length scale is imposed. This minimizes the sensitivity of the model to the inflow length scale and therefore the inflow dissipation rate prescription. The dissipation rate equation is modified near the wall so that the molecular diffusion and the destruction terms balance each other uniformly as the wall is approached. A new f_μ function is prescribed that is consistent with the limiting behavior of k and ϵ near the wall. Alternate boundary conditions on ϵ have been derived.

The low Reynolds number turbulence model together with an existing curvature correction appropriate to spinning cylinder flows has been used to simulate the flow in a U-bend with the same radius of curvature as the Space Shuttle Main Engine (SSME) Turn-Around Duct (TAD). The present computations indicate a space varying curvature correction parameter as opposed to a constant parameter as used in the spinning cylinder flows. The predictions show high levels of turbulence on the concave wall as expected. Comparison with limited available experimental data is made. The comparison is favorable, but detailed experimental data is needed to further improve the curvature model.

INTRODUCTION

The numerical solution of turbulent flow in internal flow systems is becoming increasingly necessary both as a pre-design and a post-design engineering tool. Amongst numerous flow applications, the internal flow in a duct with a sharp curvature has been one of the most difficult to handle. One of the main reasons for this difficulty is a paucity of the appropriate experimental data and the lack of appropriate turbulence models for flows with very strong curvature effects; the two not being necessarily mutually exclusive.

Achieving a solution of turbulent flow in a 180° bend is complicated by the fact that the strain rate field undergoes drastic changes as the flow turns around the bend; faster the rate of curvature, more severe the change in the strain rates. This curvature-induced effect can be taken into account in a turbulence model by, e.g., incorporating an appropriate curvature correction term into a k - ϵ turbulence model. Various such corrections

have been proposed [1,2]. Most of these corrections owe their origin to Bradshaw's analogy [3,4] of such flows to the buoyant flows and the definition of a dimensional group called the "rotational" or "curved flow" Richardson number. Mixing length is defined to be a linear function of this rotational Richardson number and the correction term is based on this number. Some authors have incorporated the Richardson number based correction term into the turbulence kinetic energy, k, equation and others into the dissipation rate, ϵ, equation. In one such model[1], the authors define a term proportional to the angular momentum so that for a positive rate of change of angular momentum in the radial direction, the Richardson number remains positive and vice-versa. They include this term in the ϵ equation such that the dissipation rate increases near the convex wall and it decreases as the concave wall is approached. This results in an increase in kinetic energy near the concave wall and a decrease in k near the convex wall as compared with a straight channel case. This correction term involves a model parameter which appears as a coefficient and its magnitude has been validated based on the flow over spinning cylinders[1].

In this study, the curvature correction model[1] has been modified to allow for an angular variation of this constant. This is important because curvature effects start to build up as the flow turns around the bend and are not representative of the situation that exists in flow over spinning cylinders. A form of this angular variation is presented in this study. In addition, cross-flow variation of this constant from convex to concave walls is also indicated.

The k - ϵ turbulence solver[5], KEM code, is used in the present study. The curvature correction to the ϵ equation is discussed below. The KEM code is cast in generalized coordinates in three dimensions and includes the diffusion terms in all the three directions. It can be used in conjunction with a compressible or an incompressible flow solver. In the present study, it is used in conjunction with an incompressible flow solver, INS3D code[6], which has evolved from the two-dimensional[7] and axi-symmetric[8] flow solvers respectively, and is based on the concept of artificial compressibility[9]. Both KEM and INS3D codes use the approximate factorization algorithm[10]. The former solves a 2x2 system implicitly, while the latter a 4x4 system. These two codes were also used in the computation of a large separated turbulent flow region in a channel with a sudden expansion[11] and in the simulation of three-dimensional turbulent flow in the National Full-Scale Aerodynamic Complex (NFAC) Wind Tunnel Inlet[12].

TURBULENCE MODEL

The prediction of turbulent flow in complex internal flow systems has now become realizable with the advent of supercomputers. One of the pacing items in this prediction

procedure is turbulence modeling. Turbulence modeling, especially at high speeds or in internal flows, is quite complex because of the paucity of appropriate experimental data and appropriate turbulence models, the two not being mutually exclusive. In internal flows, e.g., the boundary conditions at the inflow and outflow boundaries are crucial and not easily posed. In principle, some mean profiles and some turbulence profiles have to be imposed at the inflow boundaries in internal flows especially for elliptical flow fields. The sensitivity of turbulence models on the imposed inflow conditions in such situations is significant.

Various approaches have been adopted to "close" the system of equations governing a turbulent flow-field. Algebraic models have been used with success for relatively simple flows, one or two-equation models for more complicated flow situations where large separated regions or severely strained flows exist. One popular model for internal flows is the two-equation, k - ϵ model, which has been used with some success for massively separated and curved flows. However, different k - ϵ models yield different results for the same test case. Various k - ϵ models are different from one another through either wall function or low Reynolds number formulations. Away from the walls, all these models reduce to the so called "standard" k - ϵ model. In spite of this fact, the predictions away from the walls differ for different models. One of the main reasons for this is that different models are validated with different experimental test data and since the experimental data also have some uncertainty about them, e.g., refer Sultanian et al[13], the comparison of various turbulence models is not clearly made. However, direct numerical simulation results of turbulent flow in a channel, such as those of Kim et al[14], can also be used to validate turbulence models, thus alleviating this experimental uncertainty problem. Another reason for the discrepancies in the model predictions, in the author's experience, is that different inflow boundary conditions for the transport variables, k and ϵ, are used in different models in integrating the k - ϵ system. Since k and ϵ are transport properties of the flow, their distribution throughout the flow field must be, to some exent, determined by the way they are prescribed at the inflow boundary in internal flows.

In the present study, this particular problem is addressed and a low Reynolds number model is proposed which, 1) minimizes the sensitivity of the model to the manner in which the inflow boundary condition is prescribed, and 2) yields accurate predictions of the turbulence kinetic energy, k, and its peak near the wall. The present model is validated with reliable and detailed data[15] for a channel Reynolds number of 7,700 based on the channel height and also compared with the direct numerical simulation results of Kim et al[14]. The present model partly derives from some observations based on the results from direct simulation of near-wall turbulence, see Chapman and Kuhn[16].

In most of the low Reynolds number formulations, the dissipation rate at the wall is

set to zero and the effect of non-isotropy is incorporated through the governing equation for the kinetic energy, e.g., see Patel et al[17]. So the accuracy of near-wall predictions of these models is determined by the degree of approximation of the non-isotropic dissipation rate near the wall. For example, an inaccurate slope of the k - y curve near the wall and generally an under-prediction of the peak in the kinetic energy are a common feature in the predictions of these models. On inspection of the transport equations for k and ϵ for a fuily developed turbulent channel flow, it can be observed that the turbulence profiles are strongly dependent on the Reynolds number[18]. The inflow profiles must, therefore, appear as a set of curves with Reynolds number as a parameter. Therefore, in calculating a turbulent flow at a given Reynolds number, the inflow conditions must correspond to that particular Reynolds number.

The present turbulence model has been used in the turbulence solver, KEM[5], which solves the three-dimensional transport equations for the turbulence kinetic energy k and its dissipation rate ϵ in generalized coordinates with the diffusion terms retained in all the three directions. It can be used in conjunction with any compressible or incompressible flow solver to compute the turbulent flows of interest.

The governing equations for the transport quantities of turbulence, the turbulence kinetic energy, k and the dissipation rate, ϵ, can be written in cartesian coordinates as the following 2x2 system

$$\partial_t D + (F_i - F_{v_i})_{,i} = S$$

with the turbulence kinetic energy and the homogeneous dissipation rate respectively given by

$$k = \frac{1}{2}\overline{u_i u_i} \quad \text{and} \quad \epsilon = \left(\frac{\mu}{\rho}\right)\overline{u_{i,j} u_{i,j}}$$

where the solution vector is

$$D = \begin{bmatrix} \rho k \\ \rho \epsilon \end{bmatrix}$$

the flux vectors are

$$F_i = \begin{bmatrix} \rho U_i k \\ \rho U_i \epsilon \end{bmatrix} \quad \text{and} \quad F_{v_i} = \frac{1}{Re_\infty}\begin{bmatrix} \mu_k k_{,i} \\ \mu_\epsilon \epsilon_{,i} \end{bmatrix}$$

and the source term is

$$S = \frac{1}{Re_\infty}\begin{bmatrix} P - \rho\epsilon Re_\infty - F \\ C_1 \frac{\epsilon}{k} P - C_2 f_2 \frac{\epsilon^2}{k} Re_\infty - G \end{bmatrix}$$

The kinetic energy production term due to the mean shear is given by

$$P = -\rho u_i u_j U_{i,j}$$

or by

$$P = \left[\mu_t(U_{i,j} + U_{j,i}) - \frac{2}{3}\rho k\delta_{ij}\right] U_{i,j}$$

where U_i is the mean velocity and u_i is the fluctuating velocity and δ_{ij} is the Kronecker delta. The turbulent viscosity μ_t is given by

$$\mu_t = \frac{C_\mu f_\mu \rho k^2}{\epsilon} Re_\infty$$

where C_μ is a constant and f_μ is a function that takes into account the low Reynolds number dependence of C_μ.

In the present model, the function f_μ is defined as

$$f_\mu = \frac{C_3}{y^+}\exp(-C_4 y^+) + \exp\left(\frac{-1}{C_4 y^+}\right)$$

where C_3 and C_4 are constants. The present prescription for f_μ is discussed later in the current section.

Also, $\mu_k = \mu + \frac{\mu_t}{\sigma_k}$ and $\mu_\epsilon = \mu + \frac{\mu_t}{\sigma_\epsilon}$, where σ_k and σ_ϵ, turbulent Prandtl numbers for the k and ϵ transport processes respectively, are assumed to be close to unity.

The function f_2 above takes into account the low Reynolds number dependence of the constant C_2 and is defined[19] as follows:

$$f_2 = 1.0 - \frac{0.4}{1.8}\exp\{-(R_T/6)^2\}$$

The coefficient of viscosity μ is normalized by μ_∞, velocities are normalized by U_∞, distances by a characteristic length L, and the density ρ by ρ_∞. This results in the reference Reynolds number definition as

$$Re_\infty = \frac{\rho_\infty U_\infty L}{\mu_\infty}$$

The turbulent kinetic energy k is normalized by U_∞^2 and the dissipation rate ϵ is normalized by U_∞^3/L.

The equations for k and ϵ used here are applicable for both high and low turbulent Reynolds number

$$R_T = \frac{\rho k^2}{\mu\epsilon} Re_\infty$$

Values of various "constants" are chosen as follows:

$$\sigma_\epsilon = 1.3 \qquad C_3 = 12.0$$
$$\sigma_k = 1.0 \qquad C_4 = 0.05$$
$$C_1 = 1.275 \qquad C_\mu = 0.09$$
$$C_2 = 1.8$$

The values of C_1 and C_2 are inferred[19] respectively from grid turbulence data and the requirement of consistency with the von Karman constant, $\kappa = 0.42$.

For the high Reynolds number form using wall functions as boundary conditions for k and ϵ, the terms F and G are set to zero in the k- and $\epsilon-$ equations respectively. To incorporate the low Reynolds number effects, the high Reynolds number form of the k-ϵ system is modified in the present study as follows. The viscous diffusion of k and ϵ is included in the governing equations. An appropriate term G is incorporated in the ϵ equation, but the term F in the k equation is set to zero. This is different than the formulation used by Jones and Launder[20,21] and Chien[22], where they set the term F equal to the value of the near-wall non-isotropic dissipation rate and then set the boundary condition, $\epsilon = 0$ at the wall. The form of F is different in the two models[20-22]. However, since the differential equation for k involves the homogeneous dissipation rate and not just the isotropic dissipation rate, see, e.g., Hinze[23], it is more appropriate to treat ϵ as the homogeneous dissipation rate and set the boundary condition on ϵ at the wall corresponding to the non-isotropic part of the energy dissipation rate since its isotropic component reduces to zero at the wall. This boundary condition and the term G are found by using a Taylor series expansion procedure as follows.

The three fluctuating velocity components close to the wall can be expressed as

$$u = a_1 y + a_2 y^2 + a_3 y^3 + \ldots$$

$$v = b_2 y^2 + b_3 y^3 + \ldots$$

and

$$w = c_1 y + c_2 y^2 + c_3 y^3 + \ldots$$

where $a_n, b_n, c_n, n = 1,2,3$ are functions of x, z and t, so that the turbulence kinetic energy near the wall is given by

$$k = \frac{1}{2}\left[(\overline{a_1}^2 + \overline{c_1}^2)y^2 + 2(\overline{a_1 a_2} + \overline{c_1 c_2})y^3 + O(y^4)\right] \qquad (1)$$

and assuming streamwise and spanwise homogeneity near the wall, the dissipation rate near the wall is given by

$$\epsilon = \nu \left[(\overline{a_1^2} + \overline{c_1^2}) + 4(\overline{a_1 a_2} + \overline{c_1 c_2}) y + O(y^2) \right] \tag{2}$$

Since the isotropic dissipation rate at the wall reduces to zero, the wall dissipation rate is entirely the non-isotropic component and it is given by

$$\epsilon_w = 2\nu \frac{k}{y^2}$$

The zeroth order expression for the near-wall dissipation rate, $\epsilon = 2\nu \frac{k}{y^2}$, which is in error by O(y), replaces the term F in an earlier formulation[22]. However, in another formulation[20,21], the term F is expressed as

$$2\nu \left(\frac{\partial \sqrt{k}}{\partial y} \right)^2 + O(y^2)$$

which is a first order accurate expression for ϵ. Either of the preceding two expressions for ϵ can be used as a boundary condition for the dissipation rate at the wall. However, the former is more in the spirit of Dirichlet prescription and is more stable than the latter as experienced by the author[5,11]. An alternate first order accurate expression for ϵ in terms of ϵ_w has been derived[4] and it is given by

$$\epsilon_P = 4\nu \frac{k_P}{y_P^2} - \epsilon_w + O(y^2)$$

where P is a point sufficiently close to the wall. In their computations, Chapman and Kuhn[10] found that the resulting expression for the wall dissipation rate, ϵ_w, given by $4\nu \frac{k_c}{y_c^2} - \epsilon_P$ varies only slightly upto $y^+ \approx 1$ and, therefore, they suggest that this boundary condition should be used when P is within $y^+ \approx 1$. The boundary condition, $\epsilon_w = 2\nu \frac{k_c}{y_c^2}$, as used in Refs. 5 and 11, is also applied for $y^+ \approx 1$. Combining the two, upto $y^+ \approx 1$, $\epsilon_P \approx 2\nu \frac{k_c}{y_c^2}$. Now, from the expression for k given above (Eqn. 1), it is clear that k varies as y^2 close to the wall. However, it is not clear how close to the wall this behavior is true. Since even in the most reliable experimental study (e.g., see Ref. 15), the fluctuating velocity components are not measured below $y^+ \approx 1.5$, it is reasonable to assume that $k \propto y^2$ in the region below $y^+ \approx 1$. As shown later, this prescription does yield the correct kinetic energy variation near the wall and a near-wall behavior of Reynolds stress, $u'v'$, in qualitative agreement with that predicted by Coles[24].

The form of the term G which is dissipation like in Ref. 22 balances the molecular diffusion term near the wall. In Refs. 20 and 21, the form of G is different and this term is added to match the kinetic energy with the experimental data at $y^+ \approx 20$. In Ref. 22, it is assumed that the length scale in the sublayer is proportional to the normal distance from the wall and that $\epsilon \propto y^2$; therefore to be consistent with the Reichardt's requirement[25] that $\mu_t \propto y^3$ near the wall (see Refs. 14,16,24 for recent evidence of its validity for both streamwise homogeneous and inhomogeneous flows), a damping factor on the expression for μ_t which goes to zero at the wall linearly with y has to be incorporated.

In the present formulation, the term G in the ϵ equation is such that the dissipation like term $C_2 f_2 \frac{\rho\epsilon^2}{k} Re_\infty$ is damped by a factor proportional to y^2 so that there is an effective balance between the two leading terms in the ϵ equation near the wall , i.e., the molecular diffusion and the dissipation like terms. This is because $\epsilon \rightarrow \epsilon_w$ as $y \rightarrow 0$; ϵ_w being of the order of 1. Accordingly, the term G is given by

$$G = -C_2 f_2 \frac{\rho\epsilon^2}{k} Re_\infty \{\exp(-C_4 y^{+2})\}$$

The constants, C_3 and C_4 are chosen so that the peak in the kinetic energy matches with the experimental value (Ref. 15). Their relative magnitudes are chosen so that the peak in the kinetic energy is located at the position given by the experiment (Ref. 15). It should be noted here that these constants are also tied to the type of the ramp function used for the length scale at the inflow boundary although the ramp function dependence of the present model is weaker than that of the other models[20-22], as discussed in the section on Results and Discussion.

Since the turbulent viscosity is given by $\mu_t = C_\mu f_\mu \frac{\rho k^2}{\epsilon}$, and very near the wall, $k \propto y^2$ and $(\epsilon - \epsilon_w) \propto y$, the function f_μ has been constructed so that it behaves as $\frac{1}{y}$ very near the wall, (also see Ref. 16), which ensures the satisfaction of Reichardt's requirement. Away from the wall, the function f_μ tends to 1.

With this low Reynolds number form thus built into the k - ϵ system, the governing equations can be solved subject to the boundary conditions applied at the wall. Before finite differencing the equations, they are re-cast in the generalized coordinate system. Using the generalized coordinate transformation,

$$\tau \equiv t$$

$$\chi_j \equiv \chi_j(x_i, t)$$

where $\chi_j = (\xi, \eta, \zeta)$ and $x_i = (x, y, z)$, the k - ϵ system transforms to

$$\partial_\tau \overline{D} + \partial_{\chi_i} (\overline{F}_i - \overline{F}_{v_i}) = \frac{1}{J} S$$

where the solution vector,

$$\overline{D} = \frac{1}{J}\begin{bmatrix} \rho k \\ \rho \epsilon \end{bmatrix}$$

and the flux vectors,

$$\overline{F}_i = \frac{1}{J}\begin{bmatrix} \rho k Q_i \\ \rho \epsilon Q_i \end{bmatrix} \text{ and } \overline{F}_{v_i} = \frac{1}{J Re_\infty}\begin{bmatrix} \mu_k \nabla \chi_i . \nabla \chi_i \, \partial_{\chi_i} k \\ \mu_\epsilon \nabla \chi_i . \nabla \chi_i \, \partial_{\chi_i} \epsilon \end{bmatrix}$$

The Jacobian and the contravariant velocities are respectively given by

$$J = \frac{\partial_{\chi_i}}{\partial_{x_i}} \text{ and } Q_i = \partial_t \chi_i + U_j \partial_{x_j} \chi_i$$

Wall Boundary Conditions

There are various expressions that can be derived for the near-wall and wall dissipation rates in terms of the kinetic energy. Some of these (e.g., Refs. 5,11,16,20-22) have been discussed above. Referring to Eq. 1 and Eq. 2, we can also obtain a zeroth and a first order expression for the near-wall dissipation rate and they are given by

$$\epsilon = 2\nu \frac{\partial (k/y)}{\partial y} + O(y^2)$$

and

$$\epsilon = \nu \frac{1}{y} \frac{\partial k}{\partial y} + O(y)$$

These expressions can also be used as boundary conditions on ϵ. However, the boundary condition,

$$\epsilon_w = 2\nu \frac{k}{y^2}$$

or

$$\epsilon_w = 4\nu \frac{k}{y^2} - \epsilon + O(y^2)$$

are the most attractive since they do not involve computing any gradients and therefore are more stable.

Inflow Boundary Conditions

Since the kinetic energy is assumed to vary parabolically upto $y^+ \approx 1$, therefore, let $k = \alpha y^2$ in that region. The constant α is calculated as $\alpha = \frac{k_P}{y_P{}^2}$, where k_P is taken from experiment at a point P distant y_P from the wall corresponding to $y^+ \approx 1$. In this region, the length scale is given by $l \propto y^{3/2}$ as opposed to $l = \kappa y$ in the buffer or overlap layer. This follows from the mixing length hypothesis,

$$\mu_t = \rho l^2 |\frac{\partial U}{\partial y}|$$

and the fact that $\mu_t \propto y^3$ very near the wall. The constant of proportionality in the expression for the length scale is calculated by matching the two expressions, $l \propto y^{3/2}$ and $l = \kappa y$, at $y^+ \approx 1$. Therefore, if $l = \beta {y_P}^{3/2}$, then $\beta = \frac{\kappa}{\sqrt{y_P}}$, where y_P corresponds to $y^+ \approx 1$.

On comparing $\mu_t = \rho l^2 |\frac{\partial U}{\partial y}|$ and $\mu_t = C_\mu f_\mu \frac{\rho k^2}{\epsilon}$, we have an expression for the dissipation rate very near the wall as

$$\epsilon = C_\mu f_\mu \frac{k^2}{l^2 |\frac{\partial U}{\partial y}|}$$

The value of $|\frac{\partial U}{\partial y}|$ is the slope of the experimental curve for U vs. y, which is a straight line throughout the sublayer. This curve was extracted from the information in Figs. 3 and 4 of Ref. 15 and the values therein for u_τ and U at the centerline. Away from the wall, the dissipation rate is given by

$$\epsilon = \frac{{C_\mu}^{3/4} k^{3/2}}{l}$$

The preceding specification on l and ϵ is used to construct the inflow boundary condition on ϵ which is then fixed during the course of computations. This obviates the need for specifying a ramp function for l in the near-wall region to construct an ϵ profile unlike in the other models. This is important since otherwise the predictions (as in other models) suffer progressively as the grid near the wall is refined. In the course of the present computations, it was observed that for a given model it is the cut-off value of the length scale ramp function that determines the value of k away from the walls and at the center-line. As the slope of the l - y curve below the cut-off point is changed, this cut-off value has also to be changed to match the kinetic energy away from the wall, i.e., if the slope of the l -

y curve is increased, the cut-off value is decreased. In the present model, the predictions are seen to be less sensitive to the slope of ramp function since it is used above $y^+ \approx 1$. However, in the other models, the smaller the slope of the l - y curve is prescribed, the larger should this cut-off value be, and the peak in the kinetic energy is not matched as accurately as before.

CURVATURE CORRECTION

In the curvature model[1], the decay term, $C_2 f_2 \frac{\rho\epsilon^2}{k}$ in the ϵ equation is multiplied by $(1.0 - C_c Ri_t)$, where the rotational Richardson number, $Ri_t = \frac{k^2}{\epsilon^2}\frac{V_\alpha cos\alpha}{r^2}\frac{\partial(rV_\alpha)}{\partial r}$ and the coefficient, C_c, is a model parameter. In the study of turbulent flow over spinning cylinders[1], a constant value in the range, 0.1 - 0.2 (depending on the application), was used. In the present study, this parameter is made to vary both along the angular and crossflow directions. This form is preliminary and may need some modification when extensive experimental data are available for validation of the model. For the present study, C_c is set to 0.1 from 0^o to 45^o, to 0.2 from 45^o to 135^o and back to 0.1 from 135^o to 180^o. A dependence of this parameter on the crossflow direction is also indicated. Various linear variations from the convex to the concave walls were tried; a monotonic dependence of the solution on the magnitude of this variation was observed. Fine-tuning of this parameter will be achieved after a detailed comparison with the experimental data is made.

NUMERICAL METHOD

The k - ϵ system in generalized coordinates is integrated using the implicit noniterative approximate factorization algorithm of Beam and Warming[10]. The essential details of the scheme are given below. Before finite differencing the governing equations, the flux vector F_{v_i} is redefined as

$$F_{v_i} = \frac{1}{\rho Re_\infty}\begin{bmatrix}\mu_k(\rho k)_{,i}\\ \mu_\epsilon(\rho\epsilon)_{,i}\end{bmatrix} - \frac{1}{\rho^2 Re_\infty}\begin{bmatrix}\rho k\mu_k(\rho)_{,i}\\ \rho\epsilon\mu_\epsilon(\rho)_{,i}\end{bmatrix}$$

so that the second term is lumped explicitly with the source term, S. Writing the finite difference expression for the governing equation in generalized coordinates, we have

$$\frac{D^{n+1}}{J^{n+1}} + \Delta\tau\left[\delta_{\chi_i}\left(\overline{F}_i - \overline{F}_{v_i}\right)^{n+1}\right] = \frac{D^n}{J^n} + \frac{\Delta\tau}{J^n}S$$

where the time differencing is first-order (Euler) implicit, and the spatial derivatives are approximated by the central-differencing operator δ_{χ_i}.

Linearizing the flux vector $\overline{F}_i$ locally in time, this equation can be written as

$$\{I + J^{n+1}\Delta\tau\left[\delta_{\chi_i}\left(\overline{M}_i{}^n - \frac{\alpha}{\rho}\delta_{\chi_i}\right)\right]\}\left(D^{n+1} - D^n\right) = \frac{J^{n+1}}{J^n}\left(D^n + S\Delta\tau\right) - ID^n -$$

$$\Delta\tau J^{n+1}\{\delta_{\chi_i}[\left(\overline{F}_i{}^n - \frac{\alpha}{\rho}\delta_{\chi_i}D^n\right) + \frac{\alpha}{\rho^2}\left(\delta_{\chi_i}\rho\right)D^n]\}$$

where the Jacobian matrix of the flux vector $\overline{F}_i$ is given by

$$\overline{M}_i = (\overline{A}, \overline{B}, \overline{C}) = \partial_{\overline{D}}\overline{F}_i{}^n = \frac{1}{J^n}\begin{bmatrix} Q_i & 0 \\ 0 & Q_i \end{bmatrix}$$

$$\alpha = \frac{\Gamma}{J^{n+1}Re_\infty}\nabla\chi_i.\nabla\chi_i$$

with

$$\Gamma = \begin{bmatrix} \mu_k & 0 \\ 0 & \mu_\epsilon \end{bmatrix}$$

The right hand side of this equation is calculated explicitly, and the left-hand side can be factored approximately. Therefore, we have

$$\left[I + \Delta\tau J^{n+1}\delta_\xi\left(\overline{A}^n - \frac{\alpha}{\rho}\delta_\xi\right) + \epsilon_i\nabla_\xi\Delta_\xi\right]\left[I + \Delta\tau J^{n+1}\delta_\eta\left(\overline{B}^n - \frac{\alpha}{\rho}\delta_\eta\right) + \epsilon_i\nabla_\eta\Delta_\eta\right] \times$$

$$\left[I + \Delta\tau J^{n+1}\delta_\zeta\left(\overline{C}^n - \frac{\alpha}{\rho}\delta_\zeta\right) + \epsilon_i\nabla_\zeta\Delta_\zeta\right]\left(D^{n+1} - D^n\right) = RHS - \epsilon_e\left[\left(\nabla\chi_i\Delta\chi_i\right)^2\right]D^n$$

where ∇ and Δ are first order forward- and backward- difference operators, RHS is the right hand side of equation (4), ϵ_i is the implicit second order smoothing parameter. and ϵ_e is the explicit fourth order smoothing parameter. The smoothing terms are added to damp the high frequency oscillations in the solution which arise out of the central-diff rence approximation of the spatial derivatives.

DISCUSSION OF RESULTS

The experimental data used for validating the low Reynolds number turbulence model is that of Kreplin and Eckelmann[15]. The Reynolds number based on the channel height is 7,700. The validation data corresponds to fully developed conditions. Therefore, the computations were also carried out at the fully developed mean flow condition. Fully developed mean velocity profile was imposed throughout the computational domain from

the experiment and only the transport equations for k and ϵ were integrated. This simplifies the problem considerably in terms of validation of the turbulence model because the algorithm dependence of the mean velocity field solver is entirely eliminated.

Calculations were carried out for a coarse and a fine grid; in the former, the first point from the wall was situated at $y^+ \approx 2.0$ and in the latter, it was located at $y^+ \approx 0.1$ from the wall. This was necessary so as to check whether the model was uniformly valid as $y^+ \rightarrow 0$. The present predictions are compared with those of Jones and Launder[20,21] and Chien[22]. The results corresponding to these models were obtained using the KEM code[5] in the same fashion as the present model.

Given the turbulence model, a distribution for the length scale was specified for the ϵ prescription at the inflow boundary that would yield a k profile in best agreement with the experiment, especially the peak in the k profile. A ramp function $l = \kappa y, y \leq 0.35; l = constant, y \geq 0.35$ was used for the earlier two models[20-22] as well as the present model. This resulted in the best prediction of the peak in kinetic energy in all the three models. For simplicity, this length scale distribution will be called distribution A.

An alternative distribution for the length scale, referred to as distribution B, was prescribed as follows. A ramp function $l = 2.5y, y \leq 0.0136; l = constant, y \geq 0.0136$ was used for the model[20-21]; for the model[22], a ramp function $l = 2.5y, y \leq 0.033; l = constant, y \geq 0.033$ was used. For the present model, a ramp function, $l = 2.5y, y \leq 0.016; l = constant, y \geq 0.016$ was used.

Results corresponding to the length scale distribution A are discussed below. The results corresponding to distribution B will be discussed next via a comparison of kinetic energy predictions.

In Fig. 1, the results are shown corresponding to the coarse grid in terms of the kinetic energy variation from the wall to the center-line. The kinetic energy is normalized with respect to ${u_\tau}^2$; the friction velocity, u_τ, is fixed from the experiment. The experimental peak in $k/{u_\tau}^2$ is matched by the present model with no visible discrepancy whereas the two earlier models do not predict the peak very accurately. The slope of the k - y curve near the wall as predicted by the Jones and Launder model[20,21] matches that due to the present model because the near-wall non-isotropic dissipation rate has been approximated by a first order expression and not a zeroth order expression as in the Chien's model[22]. are in good agreement with each other. The dissipation rate profiles are shown in Fig. 2. The ϵ profile exhibits a linear behavior near the wall with the present model and ϵ attains a non-zero value at the wall while it goes to zero at the wall in the other two models. However, implicit in the ϵ profiles corresponding to the latter two models is the absence

of the near-wall non-isotropic dissipation rate.

Results corresponding to the fine grid are shown in Fig. 3 and Fig. 4, and they show a comparison among the experiment[15], the present model and Jones and Launder model[20,21]. As shown in Fig. 3, the experimental peak in kinetic energy is accurately matched by the present model, whereas the latter model underpredicts it appreciably. This shows that the present model is uniformly valid as $y^+ \to 0$. The corresponding ϵ profiles are shown in Fig. 4.

A comparison among the experimental data, direct simulation results of Kim et al[14] and the present predictions is shown in Fig. 5. The kinetic energy is plotted against the wall variable, $y^+ = \frac{yu_\tau}{\nu}$. The predictions shown correspond to the coarse grid. Since the present model is validated with the experimental data and not the direct simulation results, the agreement between the present predictions and the results from the direct simulation is not as good. For an added comparison, the near-wall prediction of the normalized Reynolds stress, - $\frac{\overline{u'v'}}{u_\tau^2}$, has been compared with that corresponding to Coles' deterministic model (see Ref. 24) which gives the Reynolds stress as

$$\overline{u'v'} = 0.00103\{\frac{yu_\tau}{\nu}\}^3 + O(y^4)$$

The Reynolds stress is plotted versus y^+ in Fig. 6. The behavior of the present predictions is in reasonable agreement with that of Ref. 24. If the model was validated with the direct simulation results of Kim et al[2], it is reasonable to expect that this Reynolds stress comparison would be better because the level of turbulence near the wall from the direct simulation is not as high as in the experiment.

The behavior of Reynolds stress is strongly dependent on the present f_μ prescription and this prescription is based on the model validation with respect to the experimental data[15]. It is also interesting to note that in the experiment[15], the viscous and the turbulent stresses become equal at $y^+ \approx 13$, and that in the present computations, the viscous stress equals the Reynolds stress, - $\overline{u'v'}$, at $y^+ \approx 11$ in the coarse grid case and at $y^+ \approx 12$ in the fine grid case.

The kinetic energy variation from the wall to the center-line corresponding to length scale distribution B is shown in Fig. 7. All the three models predict the peak very accurately. The experimental data at the center-line are matched accurately only by the present model. These predictions correspond to the coarse grid case.

Computations for turbulent flow in the curved duct have been carried out in two stages. First, an approximately fully developed two-dimensional turbulent channel flow profile at the outflow boundary was obtained by running a straight channel case at a

Reynolds number of 89,160 based on the channel height. The inflow boundary conditions for this case were taken from experiment[26]; the inflow profiles for the mean velocity and the turbulence kinetic energy were thus prescribed. In the second stage, the inflow boundary condition for the curved duct was fixed to be the same as the outflow boundary condition from the first stage of the computations for a straight channel.

The grid for the curved duct was chosen to have 99 points across its width (in the crossflow direction) and 141 points in the streamwise direction. The outflow boundary was placed about 25 duct heights downstream of the inflow boundary. The grid for the U-bend is shown in Fig. 8. The radius of curvature of the curved duct is the same as for the Space Shuttle Main Engine (SSME) Turn-Around Duct (TAD), and is given by $r_i/H = 0.5$, where r_i is the radius of the inner (convex) wall and h is the duct height.

The streamfunction contours in the U-bend are shown in Fig. 9. The separation zone on the convex wall extends from approximately the 120° location to over a duct height downstream of the 180° location. In Fig. 10, mean streamwise velocity is plotted for various angular locations from the convex to the concave walls. The flow is seen to accelerate upto slightly upstream of 90° location near the convex wall and then it starts to decelerate downstream. It eventually separates at about 120° location and reattaches over a duct height downstream of 180° location. This is in good agreement with the experimental results[27] obtained at Colorado State University.

The distribution of the turbulence kinetic energy in the U-bend is shown in Fig. 11 through the k contours. High levels of kinetic energy are seen near the concave wall especially across the separation bubble on the convex wall. Higher levels of kinetic energy are seen all around the bend from 0° to 180° on the concave wall as compared with those on the convex wall. The location of sharp gradients in the kinetic energy profiles across the duct is seen to be confined close to the wall on both sides as seen in Fig. 12. These peaks in the kinetic energy distribution represent high levels of turbulence production due to the presence of counter-rotating vortices close to the wall as seen in the case of a straight channel. Beyond this peak, away from the walls, higher levels of kinetic energy are present near the concave wall. This is due to the effect of curvature on turbulence. Since this study is only two-dimensional, no Goertler vortices are taken into account. Therefore, higher levels of energy near concave wall do not reflect any effect of Goertler vortices, but just the effect of rotational Richardson number introduced through the decay term in the ϵ equation. Generally, the level of kinetic energy near the concave wall is seen to be two to three times larger than that on the convex wall. Fig. 13 shows the variation of turbulence viscosity from convex to concave walls for various angular locations along the bend. Higher levels of turbulence viscosity are present near the concave wall. In general, the behavior of turbulence viscosity reflects that of the turbulence kinetic energy. Turbulence shear

stress profiles are shown in Fig. 14. The change in magnitude of shear stress from convex to concave walls is about an order of magnitude at, e.g., 90° and 128° locations. This order of magnitude variation of shear stress was also reported by Rocketdyne[28] in their experimental study of turbulent flow in an axisymmetric curved duct.

Skin friction on the two walls is shown in Fig. 15. Skin friction on the inner wall, C_{f_i}, shows the extent of the recirculation bubble on the convex wall. Some data points from Monson's experiment[29] conducted at NASA Ames Research Center at a Reynolds number of 10^6 based on the duct height are also plotted in Fig. 15. Since a sufficient number of data points are not available, the comparison with experiment is still preliminary. It is reasonable to expect that the peak in experimental C_{f_i} should lie between $S/(H/2) = 0.56$ and 2.16, see Fig. 15. However, this peak should be lower than the peak predicted by the computations since the Reynolds number corresponding to the computations is approximately 90,000, whereas that for the experiment is 10^6. That the peak in C_{f_i} is upstream of the start of the bend is quite interesting. It would appear from the mean velocity profiles that the skin friction on the convex wall should peak out around $\theta = 52°$ due to a sharp velocity gradient there, but the turbulence viscosity at the corresponding location is lower than that at those locations upstream of the bend and hence the shift of the peak in C_{f_i} upstream of the 52° location. This is a useful piece of information for the experimentalist who can thus look for and measure the quantities of interest accurately and efficiently. Although the flow conditions and the geometry are not the same, the behavior of C_{f_o}, skin friction on the outer wall, predicted by the present computations is similar to that shown in Fig. 10 in Ref. 30. The skin friction on the outer wall does not increase monotonically, but there is a slight jitter about some mean monotonic variation as shown in Fig. 15 and in Fig. 10 in Ref. 30. The asymptotic values of C_{f_i} and C_{f_o} do eventually approach the fully developed turbulent channel values corresponding to Re_H = 90,000.

Finally, a comparison is shown between the present two-dimensional predictions and the axisymmetric experimental data of Sharma and Ostermier[28] in Fig. 16. Although the present computations are carried out in a two-dimensional formulation and not axisymmetric, the trend in the velocity profiles predicted by the computations is in qualitative agreement with that given by the axisymmetric experiment.

CONCLUDING REMARKS

A low Reynolds number form of the k - ϵ turbulence model has been presented. The calculations were carried out by prescribing the fully developed mean velocity profile from experiment throughout the solution domain and by only solving for the turbulence quantities. This procedure eliminates the uncertainties that creep into the model predictions through the algorithm dependence of the mean flow solver. The model has been validated

with experimental data and has been evaluated with the results from the direct simulation of turbulence in a channel. The model predictions are also compared with those of earlier models.

The model predictions of the near-wall turbulence kinetic energy are in very good agreement with the experimental data. The experimental peak in the kinetic energy is matched exactly. The predictions are in reasonable agreement with the direct simulation results. The model is less sensitive to the specification of the inflow boundary condition on ϵ than other earlier models. However, there is a definite need for the upstream experimental data at the inflow boundary in terms of the turbulent kinetic energy appropriate to the particular Reynolds number of interest. Any approximations made in specifying the inflow boundary conditions will correspondingly influence the solution downstream especially when using a low Reynolds number turbulence model.

The function, f_μ, is so prescribed that the model is validated with the experimental data. Therefore, the near-wall behavior of Reynolds stress as predicted by a deterministic model is not accurately matched by that predicted by the present model. The peak in the kinetic energy is predicted accurately for both the coarse and fine grids. By refining the grid, little change in the predictions of kinetic energy was seen to occur and therefore not only is the solution grid independent but the turbulence model is uniformly valid as $y^+ \to 0$.

Alternate boundary conditions for ϵ have been derived although not used in the present calculations.

The present study also deals with the simulation of turbulent flow in a U-bend using a low Reynolds number k - ϵ turbulence model. The turbulence model includes an existing curvature correction which has been slightly modified in the present study. Detailed predictions on mean streamwise velocity, turbulence kinetic energy, skin friction, turbulent viscosity, etc., are made. The predicted results are in agreement with the physics of the problem. Some quantitative comparison is made with the available experimental data. An approach to refine the existing curvature correction model used here is presented that takes into account the dependence of the curvature parameter on the space variables.

The predictions reveal features of the flow field that can serve as a guide in fine-tuning experimental investigations of this class of flow fields. The present turbulent flow solution capability can be used in many engineering design situations such as in the Space Shuttle Main Engine (SSME) Turn-Around Duct (TAD) turbulent flow processes.

REFERENCES

1. Launder, B. E., Priddin, C. H. and Sharma, B. I., "The Calculation of Turbulent Boundary Layers on Spinning and Curved Surfaces," J. Fluids Engineering, Vol. 99, no. 1, pp. 231-239, 1977

2. Pourahmadi, F. and Humphrey, J. A. C., "Prediction of Curved Channel Flow with an Extended k - ϵ Model of Turbulence," AIAA J., Vol. 21, no. 10, pp. 1365-1373, 1983

3. Bradshaw, P., "Effects of Streamline Curvature on Turbulent Flow," NATO, AGARDograph No. 169, 1973

4. Bradshaw, P., "The Analogy Between Streamline Curvature and Buoyancy in Turbulent Shear Flow," J. Fluid Mech., Vol. 36, part 1, pp. 177-191, 1969

5. Kaul, U. K., "An Implicit Finite-Difference Code for a Two-Equation Turbulence Model for Three-Dimensional Flows," NASA TM-86752, June 1985

6. Kwak, D., Chang, J. L. C., Shanks, S. P. and Chakravarthy, S. R., "An Incompressible Navier-Stokes Flow Solver in Three-Dimensional Curvilinear Coordinate System Using Primitive Variables," AIAA J., Vol. 24, no. 3, pp. 390-396, 1986

7. Steger, J. L. and Kutler, P., "Implicit Finite-Difference Procedures for the Computation of Vortex Wakes," AIAA J., Vol. 15, no.4, pp. 581-590, 1977

8. Chakravarthy, S. R., "Numerical Simulation of Laminar, Incompressible Flow within Liquid Filled Shells," Report ARBRL-CR-00491, Rockwell International, Thousand Oaks, CA., 1982

9. Chorin, A. J., "A Numerical Method for Solving Incompressible Viscous Flow Problems," J. Computational Physics, Vol. 2, no. 1, pp. 12-26, 1967

10. Beam, R. M. and Warming, R. F., "An Implicit Factored Scheme for the Compressible Navier-Stokes Equations," AIAA J., Vol. 16, no. 4, pp. 393-402, 1978

11. Kaul, U. K. and Kwak, D., "Computation of Internal Turbulent Flow With a Large Separated Flow Region," Int. J. Numerical Methods in Fluids, Vol. 6, no. 12, pp. 927-937, 1986

PRECEDING PAGE BLANK NOT FILMED

PAGE 18 INTENTIONALLY BLANK

12. Champney, J. M., Coakley, T. J., Kwak, D. and Kaul, U. K., "Incompressible Viscous Flow Simulations of the NFAC Wind Tunnel," Final Report ATM-FR-25-012 under Contract NAS2-12187 to NASA Ames Research Center, June 1986

13. Sultanian, B. K., Neitze, G. P. and Metzger, D. E. "Comment on 'The Flowfield in a Suddenly Enlarged Combustion Chamber'," AIAA J.; Vol. 25, no. 6, pp. 893-895, 1987

14. Kim, J., Moin, P. and Moser, R., "Turbulence Statistics in Fully Developed Channel Flow at Low Reynolds Number," J. Fluid Mechanics, Vol. 177, pp. 133-166, 1987

15. Kreplin, Hans-Peter and Eckelmann, H., "Behavior of the Three Fluctuating Velocity Components in the Wall Region of a Turbulent Channel Flow," Physics of Fluids, Vol. 22, no. 7, pp. 1233-1239, 1979

16. Chapman, D. R. and Kuhn, G. D., "The Limiting Behavior of Turbulence Near a Wall," J. Fluid Mech., Vol. 170, pp. 265-292, 1986

17. Patel, V. C., Rodi, W. and Scheuerer, G., "Evaluation of Turbulence Models for Near-Wall and Low-Reynolds Number Flows," 3rd Int. Symposium on Turbulent Shear Flows, University of California, Davis, 1981, pp. 1.1-1.8

18. Daly, B. J. and Harlow, F. H., "Transport Equations in Turbulence," The Physics of Fluids, Vol. 13, no. 11, pp. 2634-2649, 1970

19. Hanjalic, K. and Launder B. E., "Contribution towards a Reynolds-Stress Closure for Low-Reynolds-Number Turbulence," J. Fluid Mechanics, Vol. 74, part 4, pp. 593-610, 1976

20. Jones, W. P. and Launder, B. E., "The Calculation of Low Reynolds Number Phenomena With a Two-Equation Model of Turbulence," Int. J. Heat Mass Transfer, Vol. 16, no. 6, pp. 1119-1130, 1973

21. Jones, W. P. and Launder, B. E., "The Prediction of Laminarization With a Two-Equation Model of Turbulence," Int. J. Heat Mass Transfer, Vol. 15, no. 2, pp. 301-314, 1972

22. Chien, Kuei-Yuan, "Predictions of Channel and Boundary-Layer Flows with a Low Reynolds Number Turbulence Model," AIAA J., Vol. 20, no. 1, pp. 33-38, 1982

23. Hinze, J. O., *Turbulence*, McGraw-Hill, 1975

24. Coles, D., "The Uses of Coherent Structure (Dryden Lecture)," AIAA paper 85-0506, 1985.

25. Reichardt, H., "Vollstandige Darstellung der Turbulenten Geschwindigkeitsverteilung in Glatten Leitungen. Z. Angew. Math. Mech., Vol. 31, no. 7, pp. 208-219, 1951

26. Kim, J., Kline, S. J. and Johnston, J. P., "Investigation of a Reattaching Turbulent Shear Layer: Flow Over a Backward-Facing Step," J. Fluids Engineering, ASME Trans., Vol. 102, no. 3, pp. 302-308, 1980

27. Sandborn, V. A., Holland, R. L. and Owens, S. F., "180 Degree, Small Radius of Curvature Water Channel: Measurements and 3-D Analysis," Fifth SSME CFD Workshop, NASA Marshall Space Flight Center, Huntsville, April 1987

28. Sharma, L. K. and Ostermier, B. J., "Turnaround Duct Turbulence Test," Test Report RSS-8741, ATU-86-5162, Rockwell International, Rocketdyne Division, May 1987; Results presented at the Fifth SSME CFD Workshop, NASA Marshall Space Flight Center, Huntsville, April 1987

29. Monson, D., "Experiment Supporting CFD Development for SSME TAD," Fifth SSME CFD Workshop, NASA Marshall Space Flight Center, Huntsville, April 1987

30. Ellis, L. B. and Joubert, P. N., "Turbulent Shear Flow in a Curved Duct," J. Fluid Mech., Vol. 62, part 1, pp. 65-84, 1974

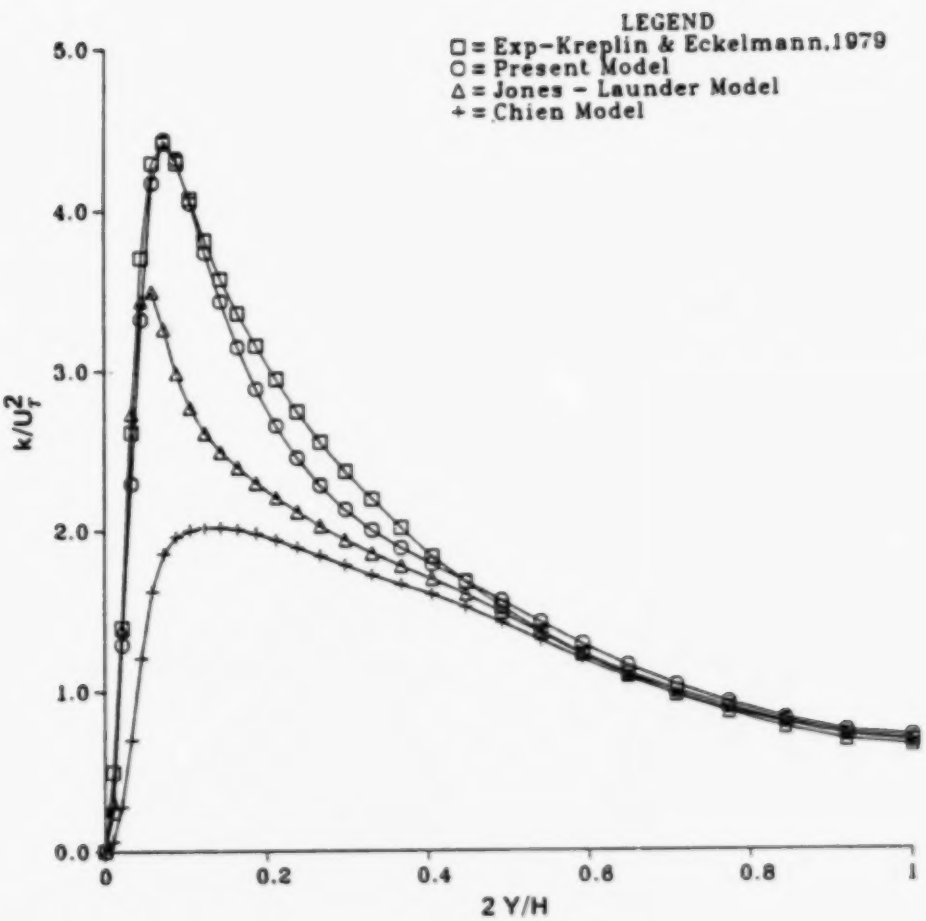

Figure 1. Variation of turbulence kinetic energy from the wall to the centerline for a coarse grid

PRECEDING PAGE BLANK NOT FILMED

PAGE 22 INTENTIONALLY BLANK

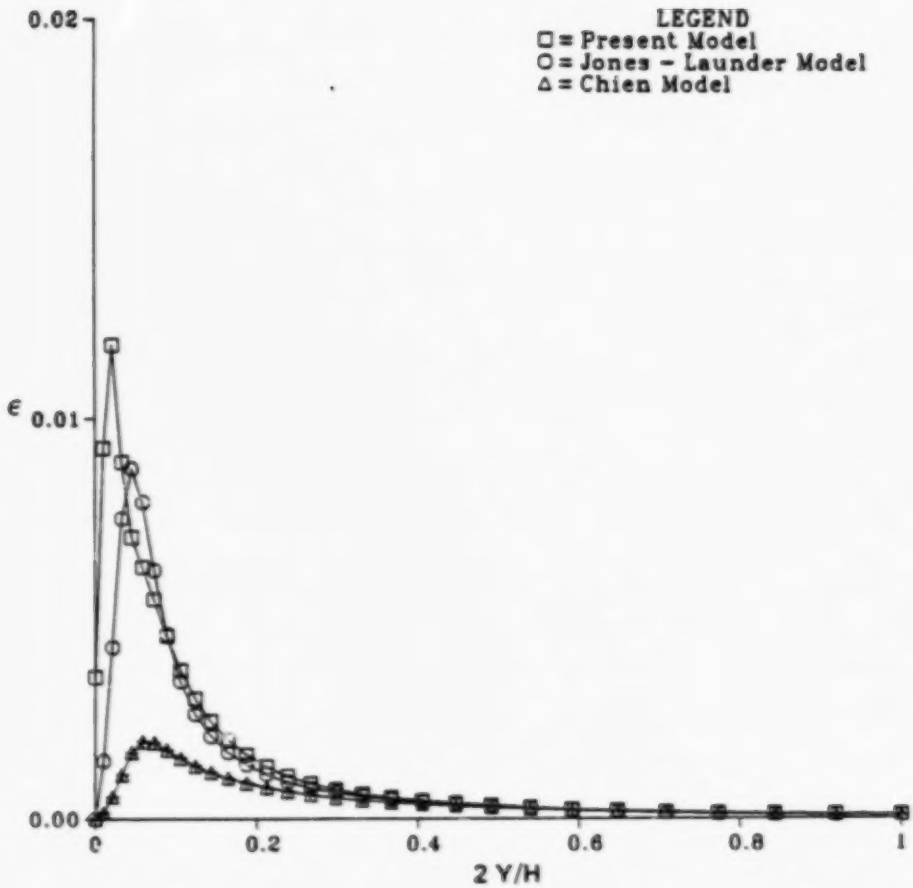

Figure 2. Variation of dissipation rate from the wall to to the center-line for a coarse grid

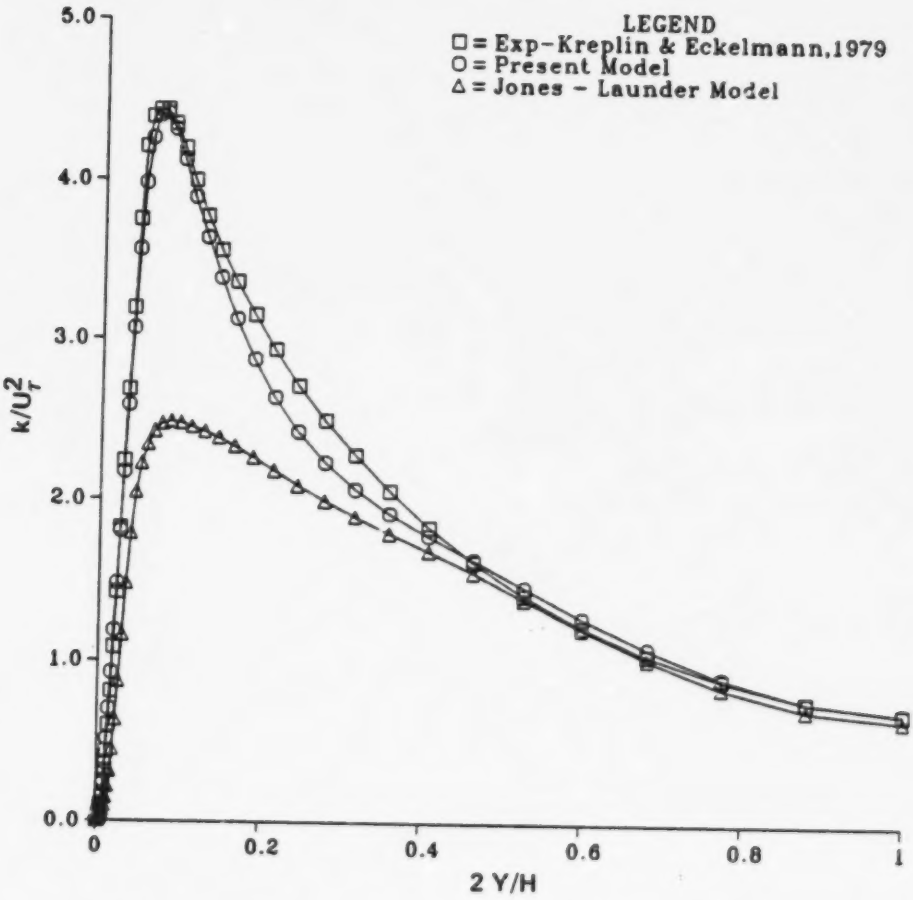

Figure 3. Distribution of turbulence kinetic energy from the wall to the center-line for a fine grid

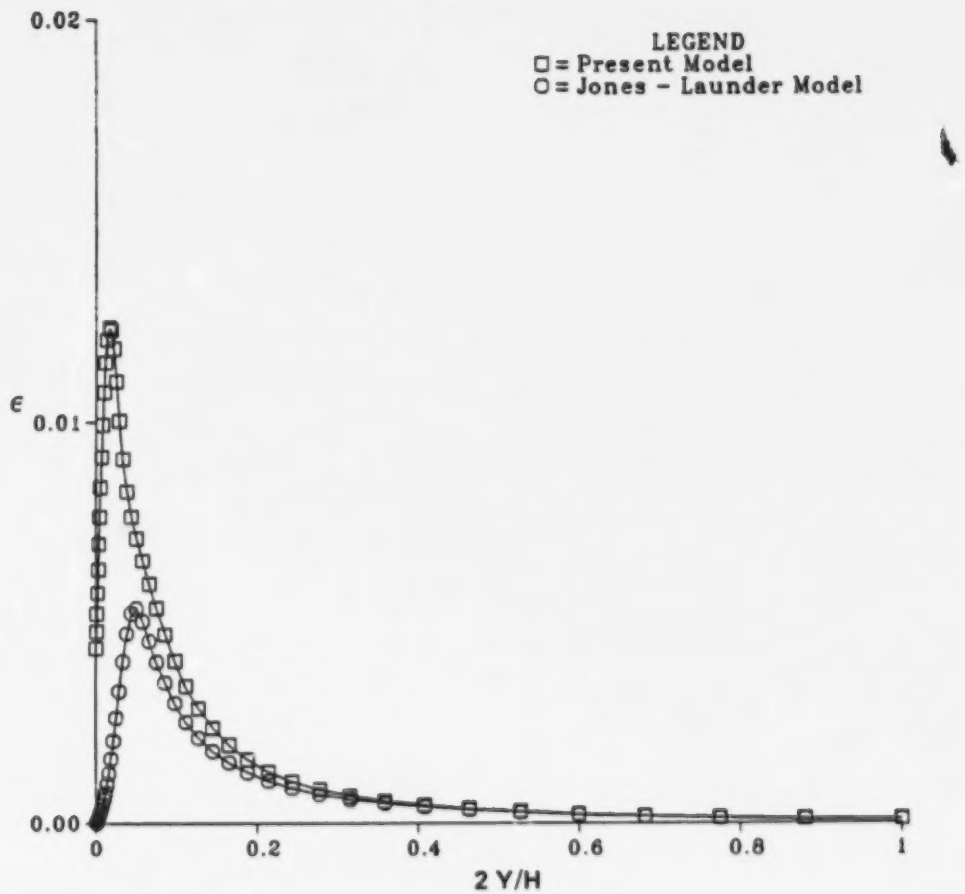

Figure 4. Distribution of dissipation rate from the wall to the center-line for a fine grid

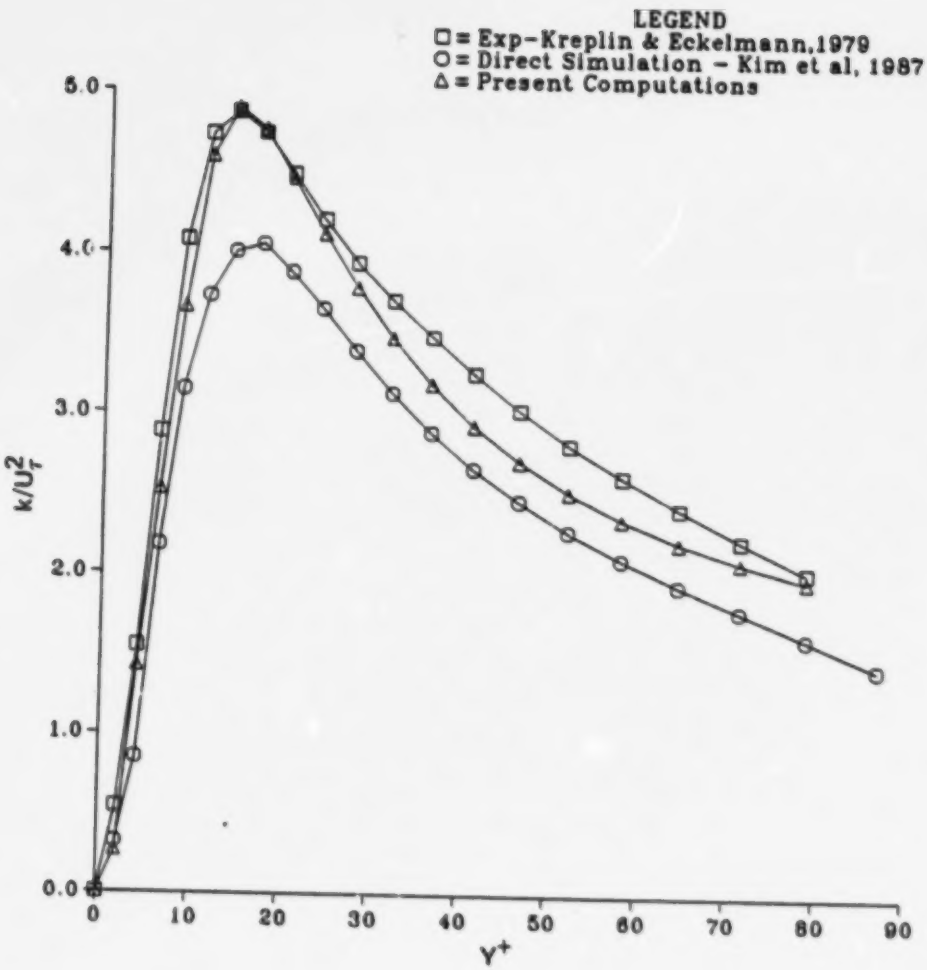

Figure 5. Near-wall variation of turbulence kinetic energy with the wall variable, y^+, for a coarse grid

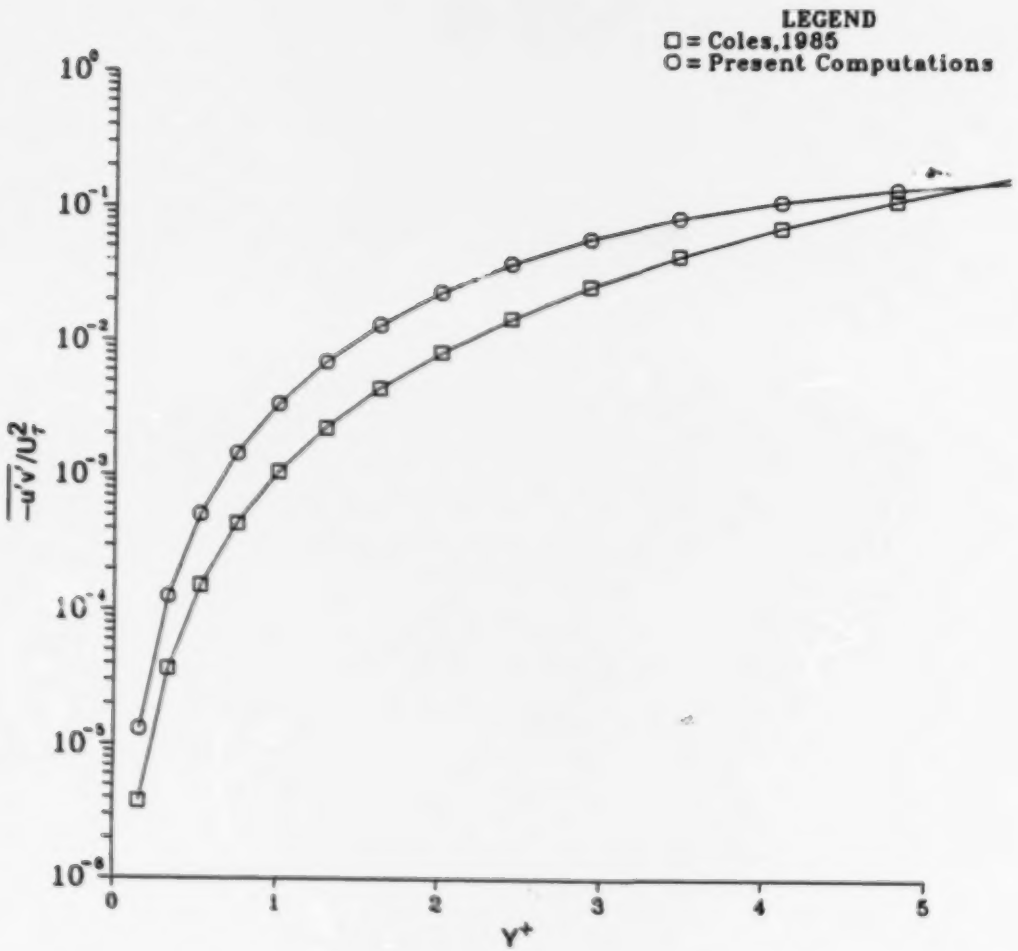

Figure 6. Near-wall variation of Reynolds stress with the wall variable, y^+, for a fine grid

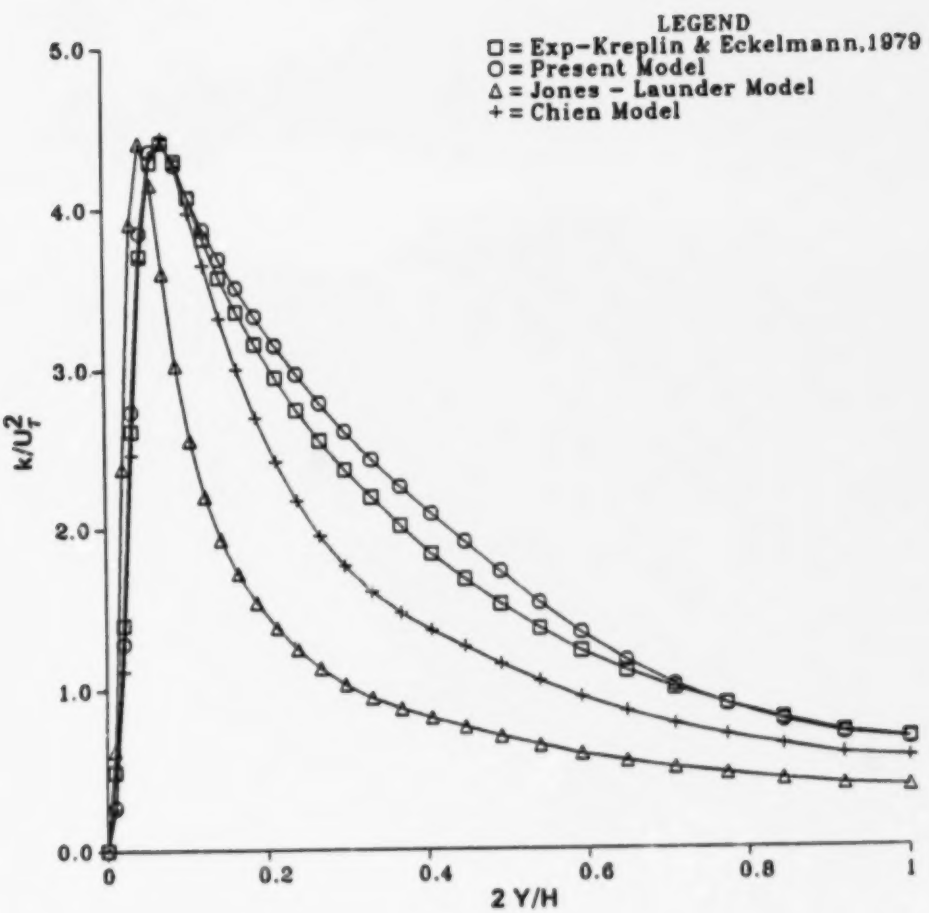

Figure 7. Distribution of turbulence kinetic energy from the wall to the center-line for a coarse grid and length scale distribution B

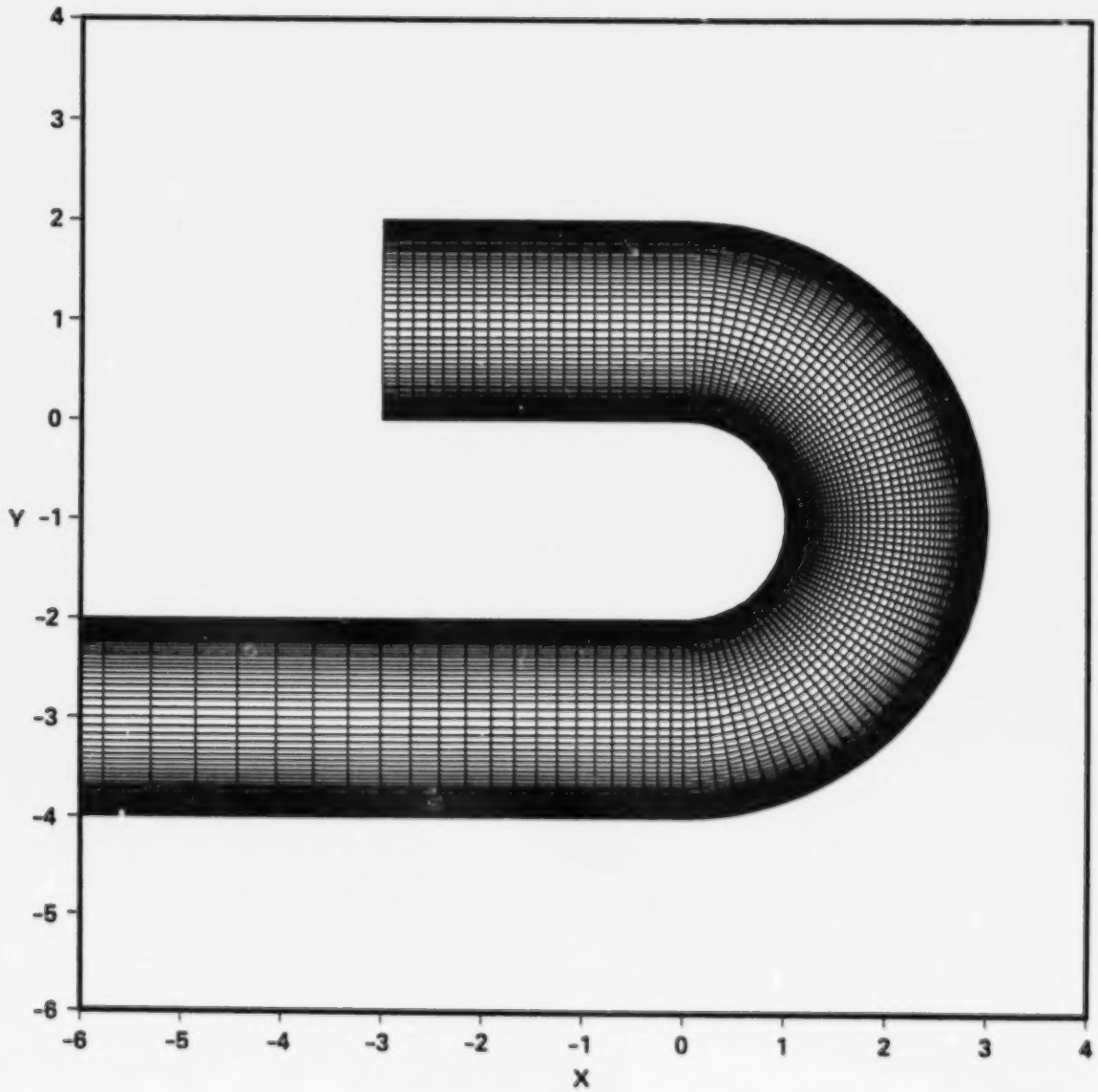

Figure 8. Grid for a Two-Dimensional U-Bend (180° Curved Duct)

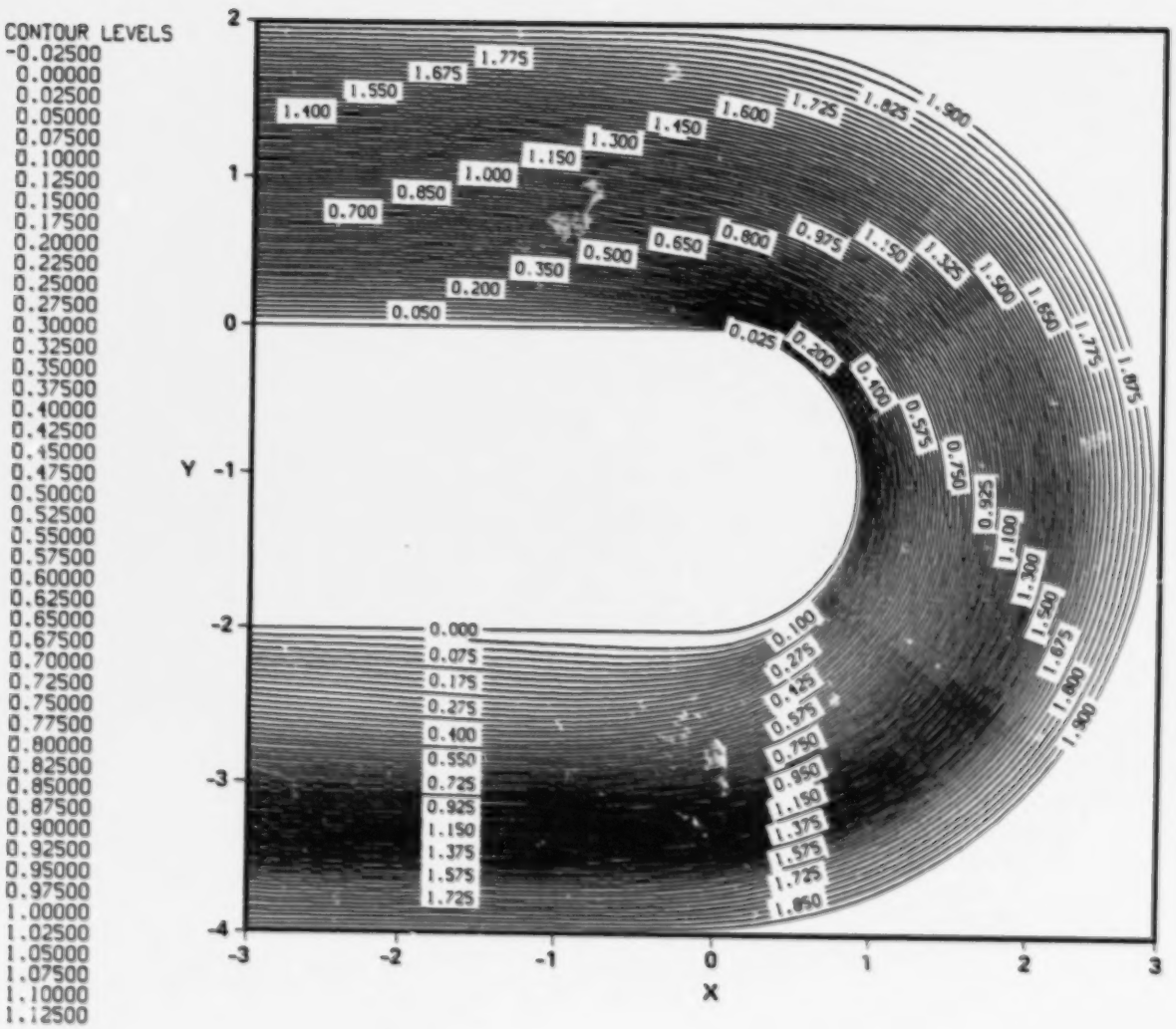

Figure 9. Streamfunction Contours in the U-Bend

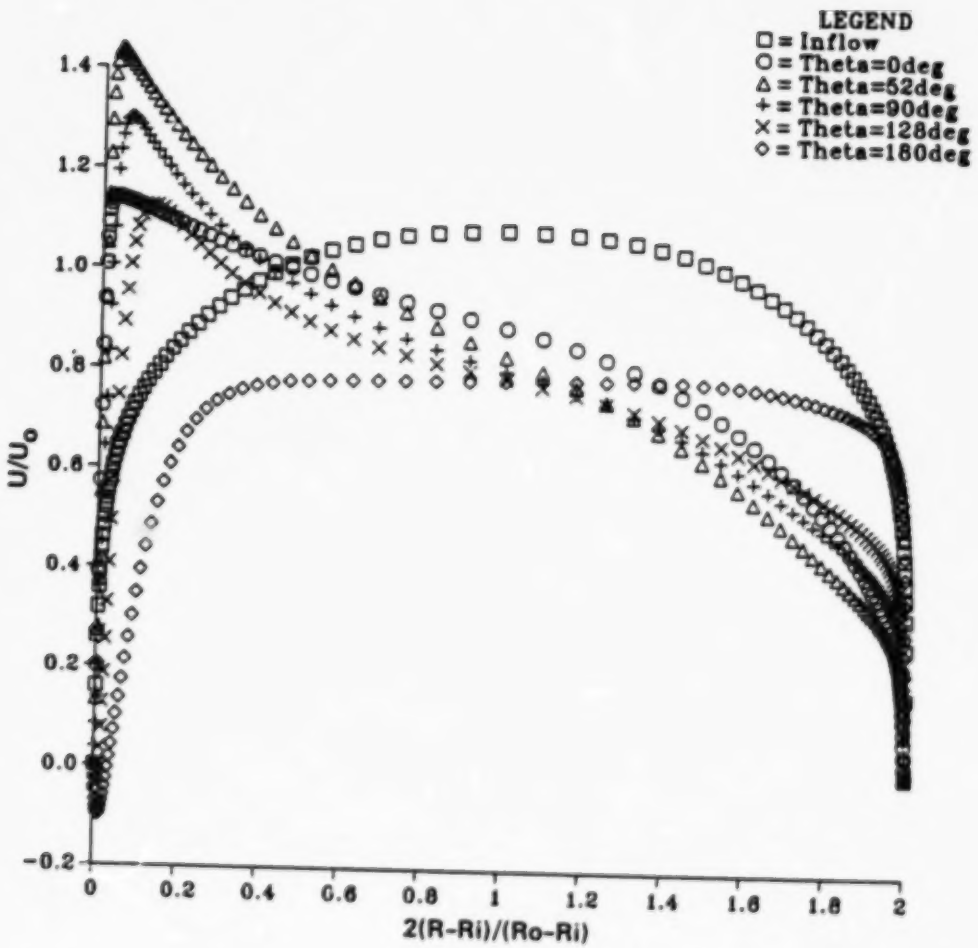

Figure 10. Cross-Flow Variation of Mean Streamwise Velocity at Various Angular Locations

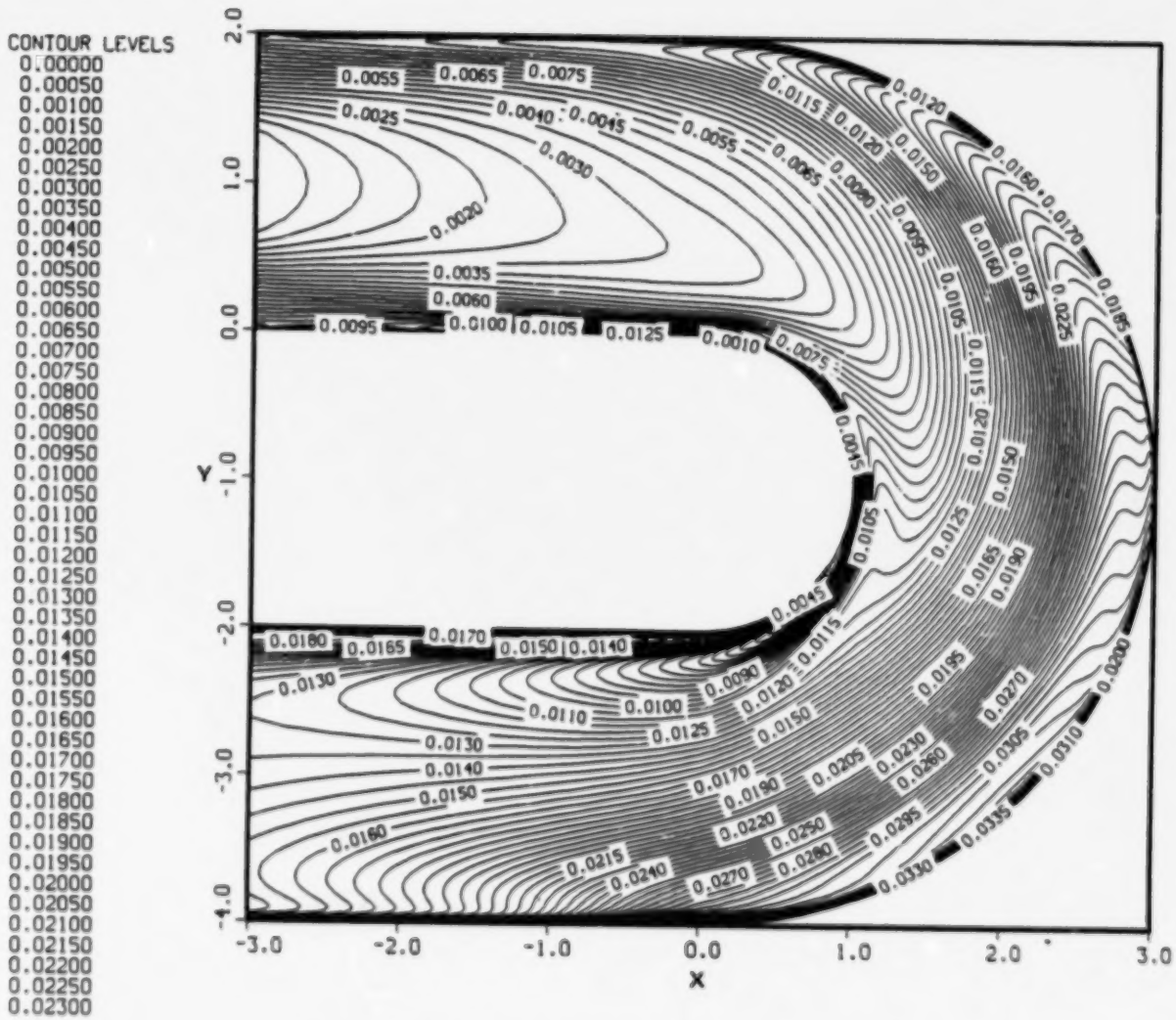

Figure 11. Turbulence Kinetic Energy Contours in the U-Bend

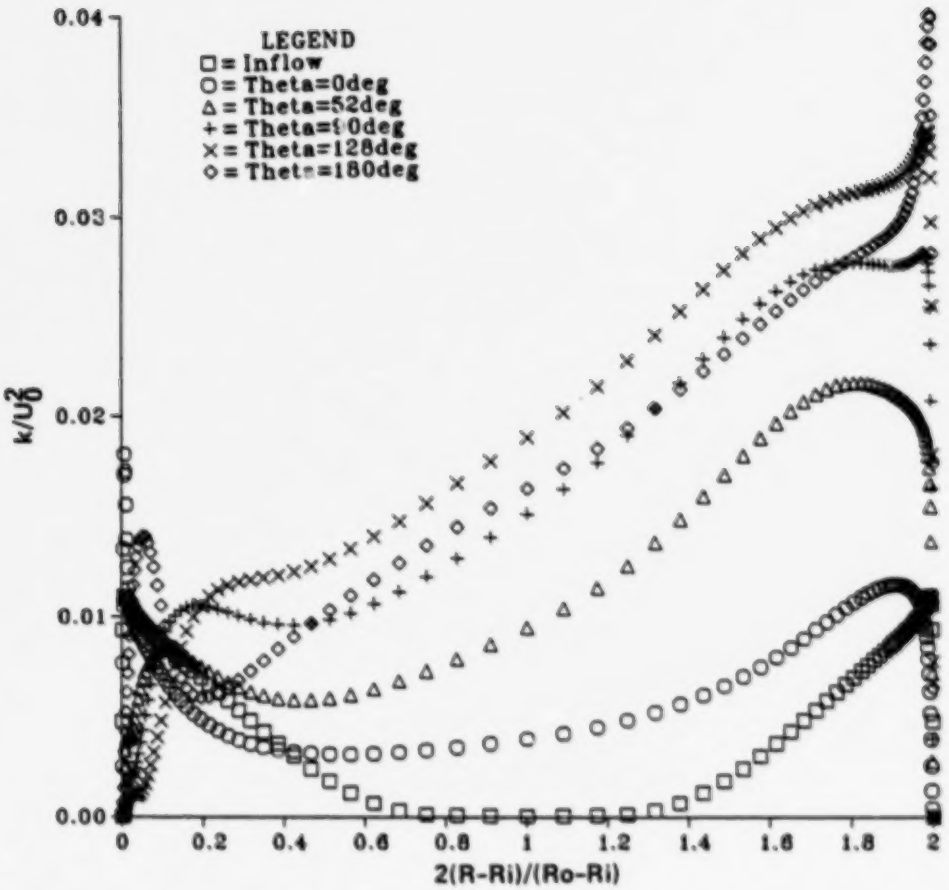

Figure 12. Cross-Flow Variation of Turbulence Kinetic Energy at Various Angular Locations

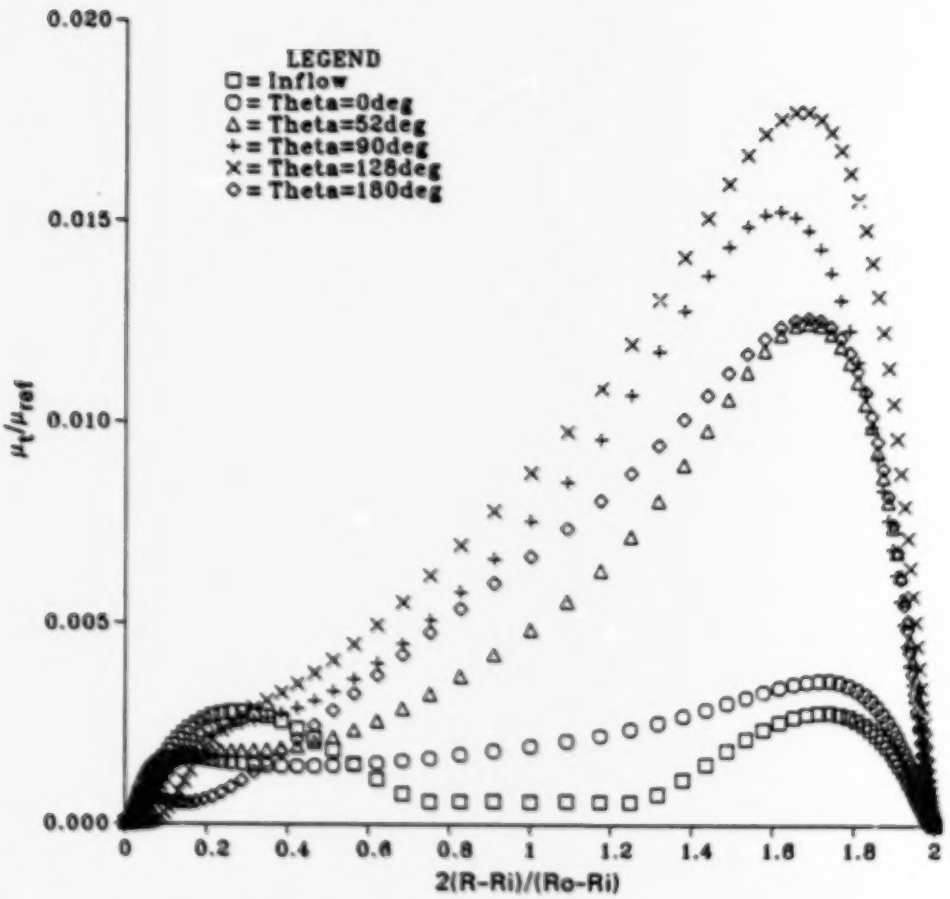

Figure 13. Cross-Flow Variation of Turbulence Viscosity at Various Angular Locations

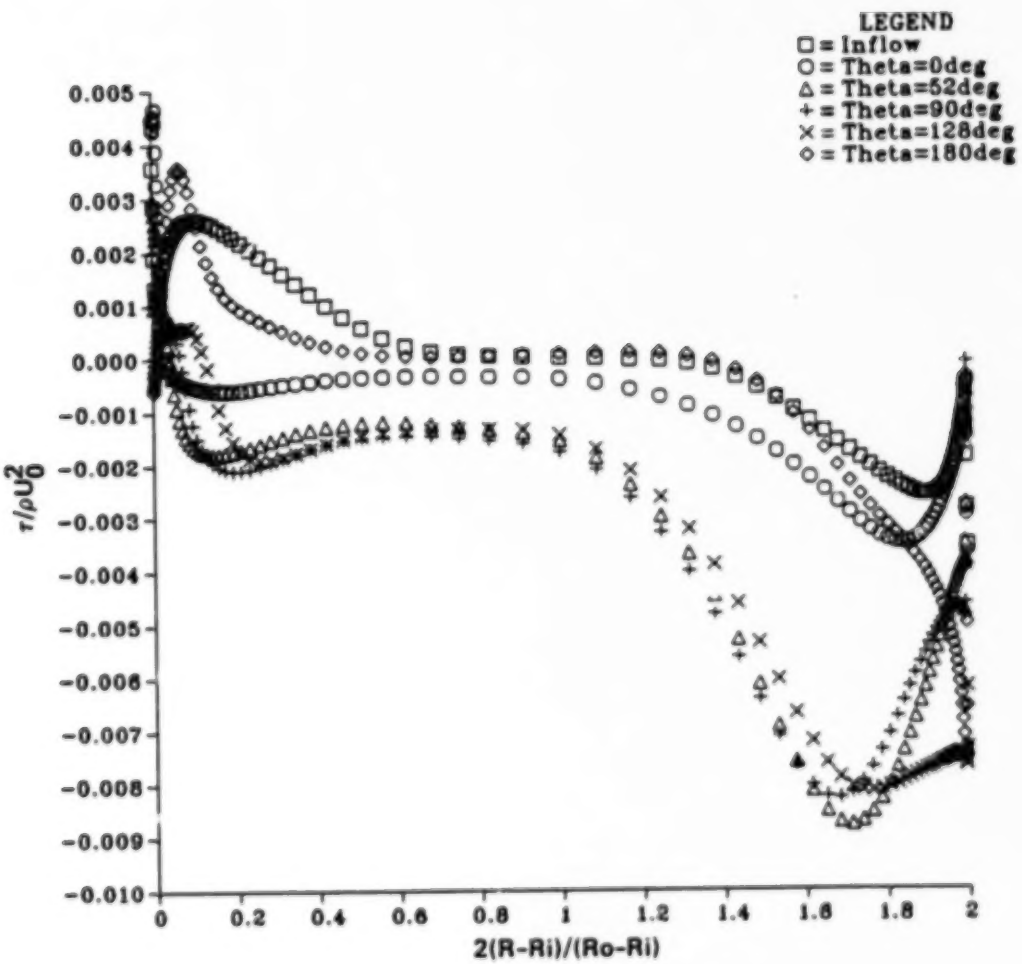

Figure 14. Cross-Flow Variation of Turbulence Shear Stress at Various Angular Locations

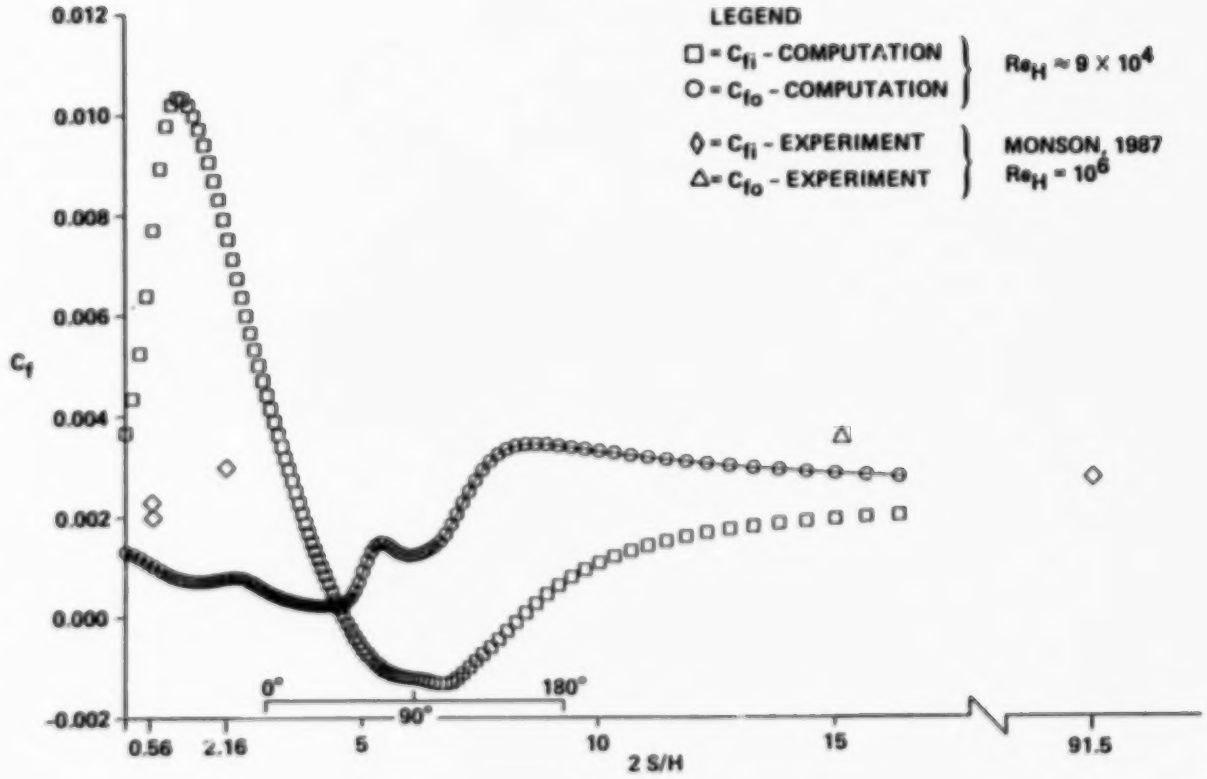

Figure 15. Variation of Skin Friction Along the Inner and Outer Walls

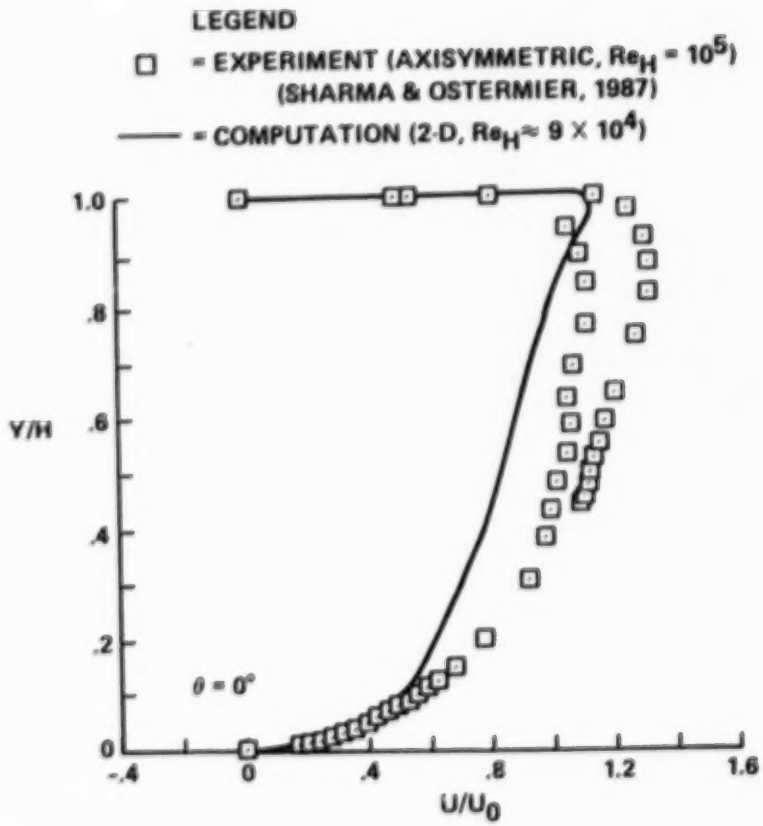

(a)

Figure 16. Comparison Between Predictions and Experimental Data for Mean Streamwise Velocity at Various Sections Around the Bend

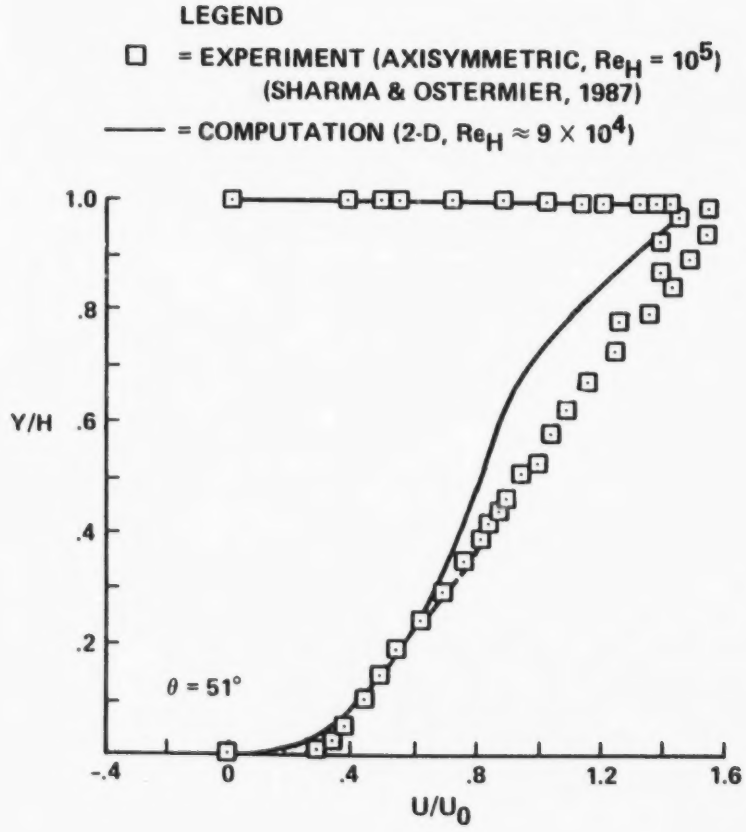

(b)

Figure 16. Continued

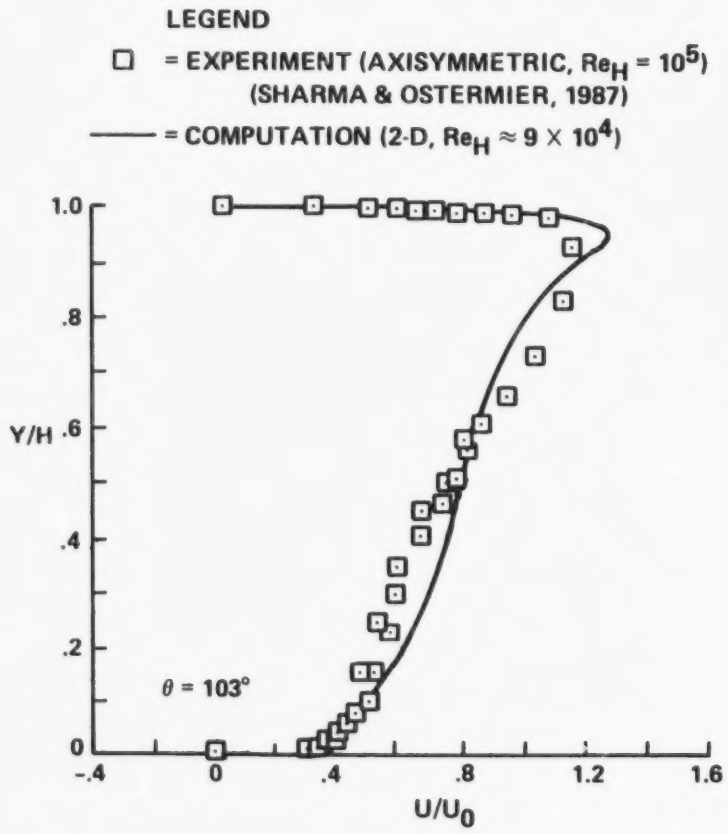

(c)

Figure 16. Continued

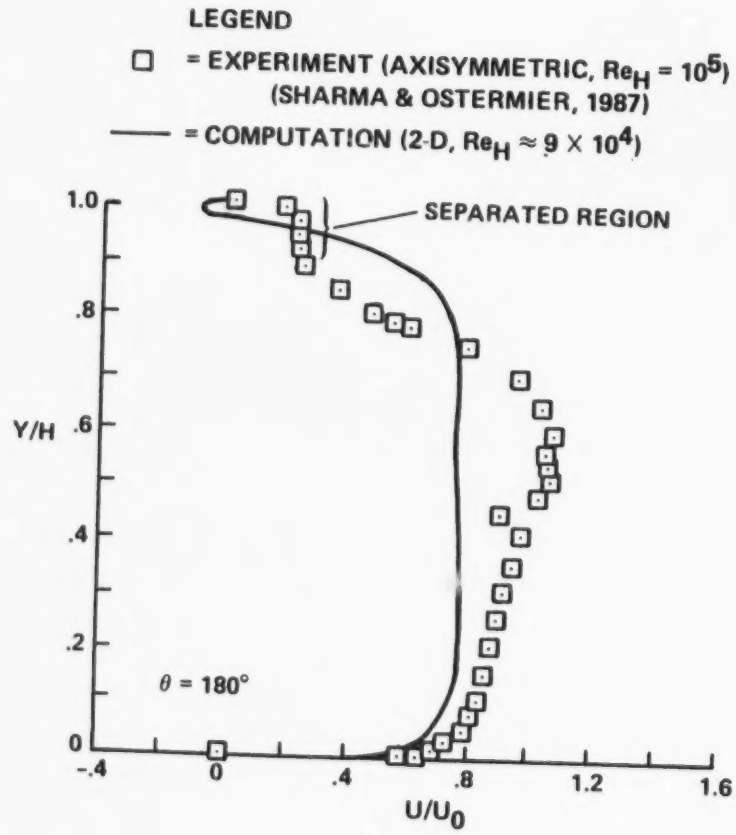

(d)

Figure 16. Concluded

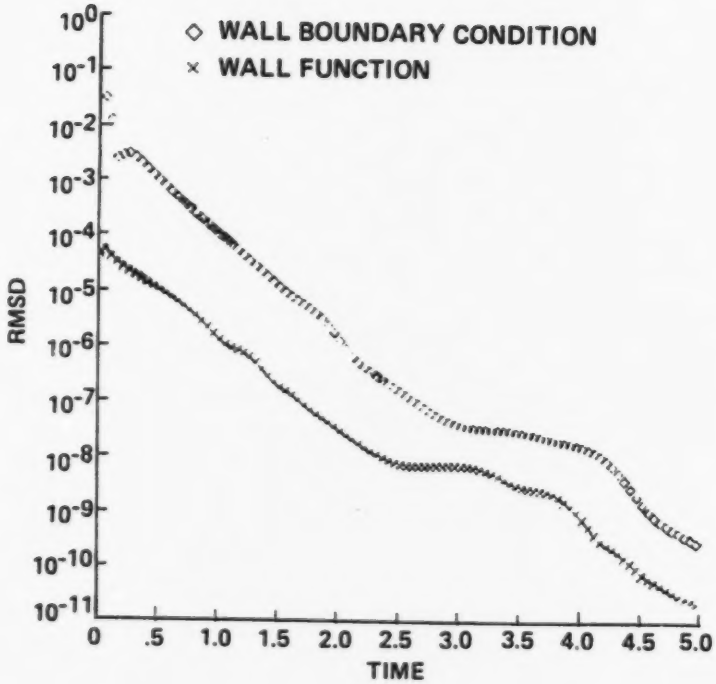

Figure A-1. Convergence History of the KEM Code Corresponding to Wall Function and Wall Boundary Condition Approaches

APPENDIX

User Manual for KEM Code

The code, KEM, has been developed in a fashion parallel to that of the AF algorithm codes developed at NASA Ames Research Center; consequently, it can easily be interfaced with any of those codes for simulating complex turbulent flows. Many of the integer parameters and counters used in the incompressible flow code, INS3D, are similarly used in KEM. There are some additional parameters used in KEM that are given default values in the initialization routine, INITKE, but are updated through the NAMELIST statement. The turbulence model constants are initialized in the routine INITKE.

A short description of each individual routine follows.

ENERGY

This routine is the main routine in the code, KEM, which is interfaced with the code INS3D, so that all the relevant parameters and variables are transferred back and forth from one to the other. The initialization routine, INITKE, is called here and the array VNUT(I) is rescaled as it is transferred from the INS3D. After VNUT(I) is updated at the end of one complete sweep in KEM, it is rescaled back to be compatible with INS3D. The routine STEPKE is called here, which is the driver routine that performs all operations necessary to update the arrays QT(1,I) and QT(2,I), ρk and $\rho\epsilon$ respectively, in the interior of the solution domain from one time step to the next. Immediately after calling STEPKE, ENERGY calls BCKE, the routine that updates the variables at the boundaries. Following this, the array VNUT(I) is calculated with the new values of ρk and $\rho\epsilon$, and the the new values of arrays, QT(1,I), QT(2,I) and VNUT(I), are printed through the routine OUTPT and stored, as and when desired.

INITKE

This is the subroutine to input data and initialize various parameters in the turbulence model. It also initializes the arrays QT(1,I), QT(2,I) and VNUT(I). It calls CHFTKE, which fits the experimental data, smoothes the data by calling SMTH, and thereby provides the inflow boundary conditions on ρk and $\rho\epsilon$. The routine INITKE then initializes the variables throughout the solution domain.

STEPKE

This driver routine performs functions in the same manner as the routine STEP in INS3D. It calls RHSKE, which calculates the right hand side of the $\rho k - \rho\epsilon$ system of equations and thereby updates the arrays ST(1,I) and ST(2,I). Then it calls the routines, FLTRKT and BLTR2, which accomplishes the matrix inversion in the K-direction of the approximate factorization algorithm and thereby the array ST is updated. The routines PBLTR2 and BLTR2 accomplish the 2x2 block tri-diagonal inversion in a given direction respectively depending on whether the given direction is periodic or non-periodic. Conventionally, in both INS3D and KEM, it is the K-direction that is allowed to be either periodic or non-periodic.

Similarly, the inversions in the J- and L-directions are accomplished respectively by first calling FLTRJT and BLTR2 and thereby updating the array ST and then by calling FLTRLT and BLTR2 and then updating the arrays ST and QT.

RHSKE

This routine calculates the right hand side of the implicit $\rho k - \rho\epsilon$ system. The routines METRIC, FLUXV and VSRHST are called for each of the three J-, K- and L-directions, and respectively return the metric quantities, the inviscid flux vector and the viscous right hand side terms appropriate to the given direction. Having thus partially updated the array ST, it calls the routine SMOOKE which calculates the explicit smoothing terms and lumps them into the array ST. Finally, the routine SOURCE is called which calculates the source terms in the $\rho k - \rho\epsilon$ system and thereby updates the array ST.

FLUXV

This routine calculates the inviscid flux vector of ρkU and $\rho\epsilon U$ for the J-direction, ρkV and $\rho\epsilon V$ for the K-direction and ρkW and $\rho\epsilon W$ for the L-direction; U, V and W are the corresponding contravariant velocities.

VSRHST

This routine calculates the viscous terms of the right hand side completely locally for all of the three co-ordinate directions. The density terms corresponding to the compressible flow fromulation are also calculated here. The array ST is thereby updated in this routine.

SMOOKE

This routine adds the explicit smoothing terms to the right hand side of the $\rho k - \rho\epsilon$ system corresponding to each of the three directions. All the calculations are done locally. The array ST is returned to the calling routine RHSKE.

SOURCE

This routine is called by RHSKE at the end. All the calculations are done locally. Most of the effort is expended in computing the appropriate metric terms in the three directions. However, if the metric quantities were to be calculated initially and stored for future use, the additional expense of having to calculate the metric terms in SOURCE would be avoided. The array ST is updated and returned to RHSKE.

FLTRJT, FLTRKT, FLTRLT

These routines fill the 2x2 blocks AT, BT and CT of the tri-diagonal matrix in each of the three co-ordinate directions by calling METRIC and AMATX corresponding to the appropriate direction. The implicit smoothing terms are also included in the arrays AT, BT and CT.

AMATX

The Jacobian matrix of the flux vector is computed here corresponding to a given direction and the array AT is returned to the appropriate calling routine.

BCKE

This routine imposes the appropriate boundary conditions. The wall function formulation is used if the logical variable, IWAL, is defined to be .TRUE. through the NAMELIST statement; otherwise, the low Reynolds number formulation is used. All the calculations are done locally for the latter case; in the former case, the routine LOGLAW is called which iteratively calculates the friction velocity, VTAU.

LOGLAW

The friction velocity, VTAU is calculated here iteratively and the array VTAU is returned to BCKE after having converged to within a specified tolerance.

BLTR2 (PBLTR2)

This routine accomplishes the inversion of tridiagonal system of 2x2 block matrices corresponding to each of the three coordinate directions, (for periodic K-direction PBLTR2 is called), and returns the solution vector F to the calling routine STEPKE. The routine LUDEC2 is called here.

LUDEC2

This routine computes the L - U decomposition elements. Block inversions in the routine BLTR2 (PBLTR2) use non-pivoted L-U decomposition.

OUTPT

The indices I, J, K and L, and arrays QT(1,I), QT(2,I), VNUT(I), Q(N,I), X(I), Y(I), Z(I) and VNUT(I) are printed for a given co-ordinate direction. This routine is called by ENERGY when NTIME equals NPRNT.

There are some default parameters that are set in the INITKE routine that can be conveniently over-ridden through a NAMELIST statement in INITKE and then assigning the new values to them at the end of the source code. These parameters are listed below.

NAMELIST/DATAKE/DISKEN, IWAL, JOFF, KOFF, LOFF,
SMUK. SMUIMK

The first two parameters DISKEN and IWAL are defined to be logical. DISKEN is .TRUE. for a restart run, and in that case, a stored solution for the arrays QT and VNUT is read in ENERGY. If IWAL is .TRUE., then the wall function formulation is used in BCKE. The parameters JOFF, KOFF, LOFF, are set to zero if IWAL is .FALSE.; otherwise, appropriate values are given them, depending on how far away from the walls the wall functions are prescribed. The wall function formulation is tested out for KOFF .NE. 0; the other two directions have not been tested yet. The parameters SMUK and SMUIMK respectively are the explicit and implicit smoothing parameters.

Sample Problems

Amongst other applications, the k - ϵ turbulence model was used to compute the turbulent flow in a channel and a duct; the KEM code contains these two options. For

simplicity, the side-wall boundary conditions for the duct are taken corresponding to those of a symmetry plane. The computational mesh used is a Cartesian grid system which is stretched in streamwise and crossflow directions. The k - ϵ solver, KEM, is made to lag the INS3D flow solver by one time step. To test the convergence property of the turbulent flow solver, a known, fully developed turbulent channel velocity profile was imposed and the k - ϵ solver was iterated to produce a converged solution of the k - ϵ system by switching off the INS3D. The convergence history is shown in Fig. A-1, where the root-mean-square values of the change in the solution vector from one time step to another is plotted against the normalized time τ. These root-mean-square values are denoted by RMSD. A comparison is made between the wall boundary condition and the wall function approach. The wall function approach exhibits superior convergence characteristics. However, both wall boundary condition and wall function approaches yield a very fast convergence on the k - ϵ solution as shown by the RMSD plots.

NASA National Aeronautics and Space Administration

Report Documentation Page

1. Report No.	2. Government Accession No.	3. Recipient's Catalog No.
NASA CR-4141		

4. Title and Subtitle	5. Report Date
Turbulent Flow in a 180° Bend: Modeling and Computations	February 1989
	6. Performing Organization Code

7. Author(s)	8. Performing Organization Report No.
Upender K. Kaul	
	10. Work Unit No. 505-60

9. Performing Organization Name and Address	11. Contract or Grant No.
Sterling Federal Systems, Inc. Palo Alto, CA	NAS2-11555
	13. Type of Report and Period Covered

12. Sponsoring Agency Name and Address	13. Type of Report and Period Covered / 14. Sponsoring Agency Code
National Aeronautics and Space Administration Washington, D. C. 20546	Contractor Report - Final
	14. Sponsoring Agency Code

15. Supplementary Notes

Point of Contact: Upender K. Kaul and Dochan Kwak, Ames Research Center, MS 258-1, Moffett Field, CA 94035 (415) 694-4480 or FTS 464-4480

16. Abstract

A low Reynolds number k - ε turbulence model has been presented which yields accurate predictions of the kinetic energy near the wall. The model is validated with the experimental channel flow data of Kreplin and Eckelmann. The predictions are also compared with earlier results from direct simulation of turbulent channel flow. The model is especially useful for internal flows where the inflow boundary condition on ε is not easily prescribed. The model partly derives from some observations based on earlier direct simulation results of near-wall turbulence.

The low Reynolds number turbulence model together with an existing curvature correction appropriate to spinning cylinder flows has been used to simulate the flow in a U-bend with the same radius of curvature as the Space Shuttle Main Engine (SSME) Turn-Around Duct (TAD). The present computations indicate a space varying curvature correction parameter as opposed to a constant parameter as used in the spinning cylinder flows. The predictions show a high level of turbulence on the concave wall as expected. Comparison with limited available experimental data is made. The comparison is favorable, but detailed experimental data is needed to further improve the curvature model.

17. Key Words (Suggested by Author(s))	18. Distribution Statement
Low Reynolds Number k - ε Model Curvature Correction Space Shuttle Main Engine Turn-Around Duct	Unclassified - Unlimited Subject Category 34

19. Security Classif. (of this report)	20. Security Classif. (of this page)	21. No. of pages	22. Price
Unclassified	Unclassified	56	A04